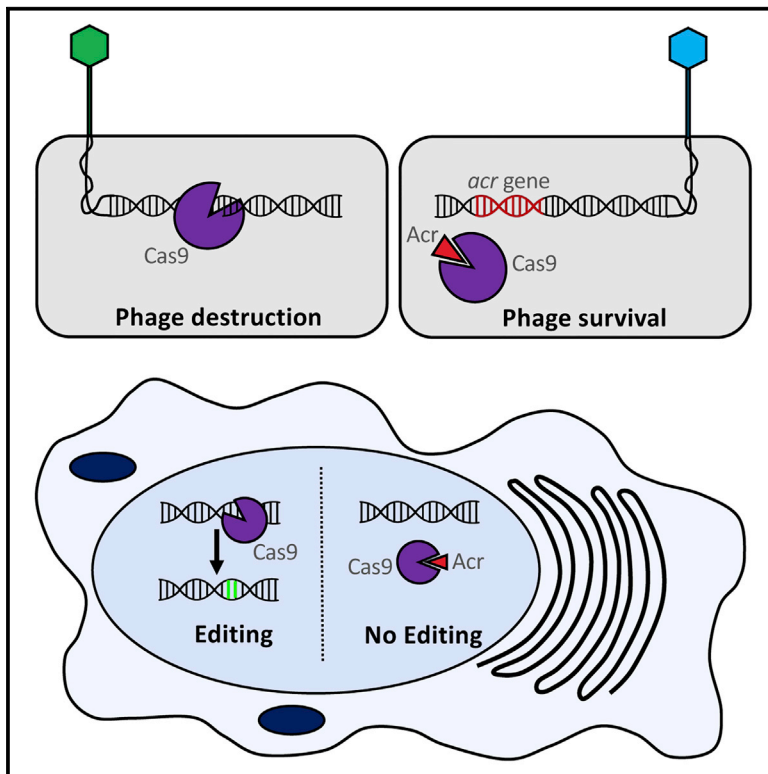


Naturally Occurring Off-Switches for CRISPR-Cas9

Graphical Abstract



Authors

April Pawluk, Nadia Amrani,
Yan Zhang, ..., Erik J. Sontheimer,
Karen L. Maxwell, Alan R. Davidson

Correspondence

erik.sontheimer@umassmed.edu (E.J.S.),
karen.maxwell@utoronto.ca (K.L.M.),
alan.davidson@utoronto.ca (A.R.D.)

In Brief

Naturally occurring inhibitors of CRISPR-Cas9 can block genome editing in cultured human cells, providing a means to spatially, temporally, and conditionally control Cas9 activity.

Highlights

- Some mobile elements in bacteria encode protein inhibitors of Cas9
- Three families of anti-CRISPRs inhibit *N. meningitidis* Cas9 in vivo and in vitro
- Anti-CRISPRs bind directly to NmeCas9
- These proteins are potent “off-switches” for NmeCas9 genome editing in human cells

Naturally Occurring Off-Switches for CRISPR-Cas9

April Pawluk,¹ Nadia Amrani,² Yan Zhang,² Bianca Garcia,³ Yurima Hidalgo-Reyes,³ Jooyoung Lee,² Alireza Edraki,² Megha Shah,¹ Erik J. Sontheimer,^{2,*} Karen L. Maxwell,^{1,4,*} and Alan R. Davidson^{1,3,5,*}

¹Department of Biochemistry, University of Toronto, 1 King's College Circle, Toronto, ON M5S 1A8, Canada

²RNA Therapeutics Institute, Program in Molecular Medicine, University of Massachusetts Medical School, 368 Plantation Street, Worcester, MA 01605-2324, USA

³Department of Molecular Genetics, University of Toronto, 1 King's College Circle, Toronto, ON M5S 1A8, Canada

⁴Donnelly Centre for Cellular and Biomolecular Research, University of Toronto, 160 College Street, Toronto, ON M5S 3E1, Canada

⁵Lead Contact

*Correspondence: erik.sontheimer@umassmed.edu (E.J.S.), karen.maxwell@utoronto.ca (K.L.M.), alan.davidson@utoronto.ca (A.R.D.)
<http://dx.doi.org/10.1016/j.cell.2016.11.017>

SUMMARY

CRISPR-Cas9 technology would be enhanced by the ability to inhibit Cas9 function spatially, temporally, or conditionally. Previously, we discovered small proteins encoded by bacteriophages that inhibit the CRISPR-Cas systems of their host bacteria. These “anti-CRISPRs” were specific to type I CRISPR-Cas systems that do not employ the Cas9 protein. We posited that nature would also yield Cas9 inhibitors in response to the evolutionary arms race between bacteriophages and their hosts. Here, we report the discovery of three distinct families of anti-CRISPRs that specifically inhibit the CRISPR-Cas9 system of *Neisseria meningitidis*. We show that these proteins bind directly to *N. meningitidis* Cas9 (NmeCas9) and can be used as potent inhibitors of genome editing by this system in human cells. These anti-CRISPR proteins now enable “off-switches” for CRISPR-Cas9 activity and provide a genetically encodable means to inhibit CRISPR-Cas9 genome editing in eukaryotes.

INTRODUCTION

CRISPR-Cas9-mediated genome editing has revolutionized biotechnology and holds immense promise for therapeutic applications. Cas9 is a nuclease that can be programmed with a guide RNA molecule to cut nearly any desired DNA sequence (Gasiunas et al., 2012; Jinek et al., 2012), enabling mutagenesis or editing at the site of cleavage (Cho et al., 2013; Cong et al., 2013; Hwang et al., 2013; Jiang et al., 2013; Jinek et al., 2013; Mali et al., 2013). This RNA-guided DNA editing technology is being developed for personalized gene therapy to correct inherited disease, for sequence-specific targeting of pathogens to treat infectious disease, and many other applications (Bikard et al., 2014; Ebina et al., 2013; Gomaa et al., 2014; Kaminski et al., 2016; Ousterout et al., 2015; Wu et al., 2013; Yin et al., 2014).

Although the utility of Cas9 DNA targeting is widely acknowledged, there are currently limited means to exert control over Cas9 activity once it has been activated or delivered, leading

to practical difficulties and safety concerns. For example, off-target effects (cleavage and mutation at unintended, near-cognate genomic sites) are exacerbated by excessive or prolonged Cas9 activity (Fu et al., 2014; Hsu et al., 2013; Pattanayak et al., 2013). Many potential therapeutic applications of CRISPR-Cas9 only require editing in specific target tissues, and Cas9 activity in ancillary tissues is at best useless and at worst a safety risk. When zygotic injections of CRISPR-Cas9 components are used to generate mutant animals (Wang et al., 2013), Cas9 activity after the initial rounds of mitosis can give rise to mosaic genotypes (Yen et al., 2014). In applications that require homology-dependent repair (HDR) for precise editing, Cas9 activity during the G1 phase of the cell cycle (when HDR pathways are suppressed) (Orthwein et al., 2015) increases the background of undesired imprecise edits. Recently, CRISPR-Cas9 gene drives (that cause desired genes to propagate throughout natural populations through non-Mendelian forced inheritance) have been developed, in part to advance the long-term goal of eradicating disease vectors such as mosquitos (Gantz et al., 2015; Hammond et al., 2016). A danger of this approach is that gene drives, once introduced into the environment, could be difficult to restrain and could have unpredictable ecological consequences. Based on these and other considerations, the performance and safety of CRISPR-Cas9 applications could be greatly improved if Cas9 activity could be more effectively controlled. Several groups have devised methods to activate CRISPR-Cas9 genome editing in response to specific cues, including light-inducible and drug-inducible Cas9 activity (Nihongaki et al., 2015; Nuñez et al., 2016; Wright et al., 2015). However, a robust, specific, and genetically encodable “off-switch” for Cas9 activity has not yet been identified.

CRISPR-Cas9 technologies are derived from type II CRISPR-Cas adaptive immune systems of bacteria, which target and destroy foreign DNA entities such as bacteriophages (phages) and plasmids (Barrangou et al., 2007; Deltcheva et al., 2011). Although the Cas9 ortholog from *Streptococcus pyogenes* strain SF370 (SpyCas9, subtype II-A) (Makarova et al., 2015) is the most commonly used and the best understood, type II CRISPR-Cas systems from several other bacterial species have also been adapted for eukaryotic genome editing (Cong et al., 2013; Esvelt et al., 2013; Hirano et al., 2016; Hou et al., 2013; Lee et al., 2016; Müller et al., 2016; Ran et al., 2015). For example, Cas9 from *Neisseria meningitidis* (NmeCas9), which

belongs to the CRISPR-Cas subtype II-C (Makarova et al., 2015), is an effective tool for human genome editing (Esvelt et al., 2013; Hou et al., 2013; Lee et al., 2016, N.A., X.D. Gao, L.J. Zhu, S.A. Wolfe, and E.J.S, unpublished data). NmeCas9 is hundreds of amino acids smaller than SpyCas9, facilitating viral delivery, and it is also less prone to off-target effects (Esvelt et al., 2013; Hou et al., 2013; Lee et al., 2016, N.A., X.D. Gao, L.J. Zhu, S.A. Wolfe, and E.J.S, unpublished data). “Dead” NmeCas9 (dNmeCas9), in which nuclease active-site residues have been mutated, has also proven to be an effective, specific RNA-guided genome binding platform (Esvelt et al., 2013; Hilton et al., 2015; Kearns et al., 2015; Ma et al., 2015b), similar to dSpyCas9 and other nuclease-inactivated orthologs (reviewed in Dominguez et al., 2016; Wang et al., 2016).

The goal of the work described here was to identify naturally occurring protein inhibitors of a CRISPR-Cas9 system. The rationale for this endeavor was our previous discovery of inhibitors of both the type I-E and type I-F CRISPR-Cas systems (Bondy-Denomy et al., 2013; Pawluk et al., 2014). These proteins, which we named anti-CRISPRs, are small proteins encoded by phages that allow a bacterial host’s CRISPR-Cas immune system to be evaded. Anti-CRISPRs function through a variety of mechanisms (Bondy-Denomy et al., 2015), and we recently discovered that multiple families of type I-F anti-CRISPRs occur widely in mobile genetic elements (MGEs) (e.g., phages and conjugative elements) of diverse bacterial species (Pawluk et al., 2016). Although type I systems use Cas proteins that are completely unrelated to Cas9, we hypothesized that inhibitors of type II systems would also exist, because they would confer strong evolutionary advantages to MGEs encoding them. Thus, we employed the same bioinformatic approach that successfully identified type I anti-CRISPRs to search for inhibitors of Cas9. As described below, this effort led us to discover three distinct anti-CRISPR protein families that potently inhibit the *N. meningitidis* type II-C CRISPR-Cas system. These proteins directly interact with NmeCas9 and can function as off-switches for NmeCas9 genome editing activity in cultured human cells.

RESULTS

Three Distinct Anti-CRISPRs Inhibit CRISPR-Cas Activity in *Neisseria meningitidis*

A conserved feature of characterized anti-CRISPR (*acr*) genes is the presence of a downstream gene encoding a putative transcriptional regulator. In previous work, we identified two distinct families of these helix-turn-helix (HTH) containing anti-CRISPR-associated (Aca) proteins, which we called Aca1 and Aca2. Identification of genes encoding Aca proteins in diverse bacterial species led us to discover five new families of type I-F *acr* genes encoded directly upstream of the *aca* genes, thereby providing precedent for the use of genomic localization to predict anti-CRISPR activity of novel, hypothetical protein families with high confidence (Pawluk et al., 2016). We reasoned that genes encoding inhibitors of type II CRISPR-Cas systems would be found upstream of *aca* genes in MGEs within species bearing type II systems. By conducting a series of BLAST searches with Aca1 and Aca2, we identified a candidate anti-CRISPR gene in a *Brackiella oedipodis* putative conjugative element

that encoded a 91-residue hypothetical protein (accession NCBI: WP_028357638.1) lying directly upstream of an *aca2* gene (Figure 1A). This putative anti-CRISPR possessed several homologs encoded in MGEs of diverse Proteobacteria and a distant, putative ortholog in a Firmicute, *Fenollaria massiliensis* (Figure S1). The most frequently observed CRISPR-Cas system among species encoding homologs of this protein was type II-C. Thus, we hypothesized that this putative anti-CRISPR family would inhibit the activity of one or more representative type II-C Cas9 orthologs. Because *N. meningitidis* strain 8013 harbors the best-established type II-C CRISPR-Cas system (Zhang et al., 2013, 2015), and because we identified a strain of *N. meningitidis* among the genomes that contain an MGE encoding a member of this putative anti-CRISPR family (Figures 1A and S1; Tables S1 and S2), we used NmeCas9 to test this hypothesis.

We measured the ability of the candidate type II-C anti-CRISPR gene from *B. oedipodis* and its 29% identical homolog from *N. meningitidis* (Figure 1A) to inhibit type II-C CRISPR-Cas activity in its native context, using a previously described natural transformation assay in *N. meningitidis* 8013 (Zhang et al., 2013, 2015). In this assay, the transformation frequency of a plasmid bearing a CRISPR-targeted protospacer sequence was compared to that of a control plasmid lacking the protospacer. We used the wild-type strain as well as isogenic derivatives with an integrated, empty *Neisseria* intergenic complementation site (*nics*) cassette, or the same cassette carrying genes encoding either of the two candidate anti-CRISPR proteins (Figure 1B), each driven by the *N. meningitidis* *cas9* promoter. In wild-type cells and the empty-vector control, robust type II-C CRISPR-Cas activity resulted in a $\geq 10^4$ -fold decrease in the transformation frequency of CRISPR-targeted DNA (Figure 1C). Strikingly, expression of the putative anti-CRISPRs resulted in equal transformation frequencies when targeted or untargeted DNA was used (Figure 1C), reflecting a lack of CRISPR interference. These data implied that the type II-C CRISPR-Cas system of *N. meningitidis* was indeed inhibited by these putative anti-CRISPR genes, which we named *acrIIC1*_{Boe} and *acrIIC1*_{Nme}. Although *acrIIC1*_{Boe} has presumably evolved to inhibit the Cas9 ortholog found in *B. oedipodis* (BoeCas9), NmeCas9 is 47% identical to BoeCas9, suggesting that this similarity is sufficient to account for the observed cross-species inhibition.

All of the identified *acrIIC1* homologs except *acrIIC1*_{Boe} were not found adjacent to *aca1* or *aca2* genes, but instead many were encoded upstream of a variety of genes encoding distinct HTH-containing proteins (Figures 1 and S1). We hypothesized that these could represent new families of *aca* genes and could therefore lead to new anti-CRISPR candidates. Using BLAST searches, we determined that homologs of the HTH protein-coding gene downstream of *acrIIC1*_{Nme} were the only putative *aca* genes found repeatedly in genomic regions displaying MGE-like properties. Of greatest interest, we identified members of this gene family in putative prophage elements in *N. meningitidis* strains, and in several cases the HTH-containing protein coding gene was immediately downstream of the same two small, uncharacterized open reading frames, neither of which exhibited detectable sequence similarity to *acrIIC1*_{Nme}. We cloned these two distinct genes and tested each one for anti-CRISPR activity. Using the *N. meningitidis* transformation

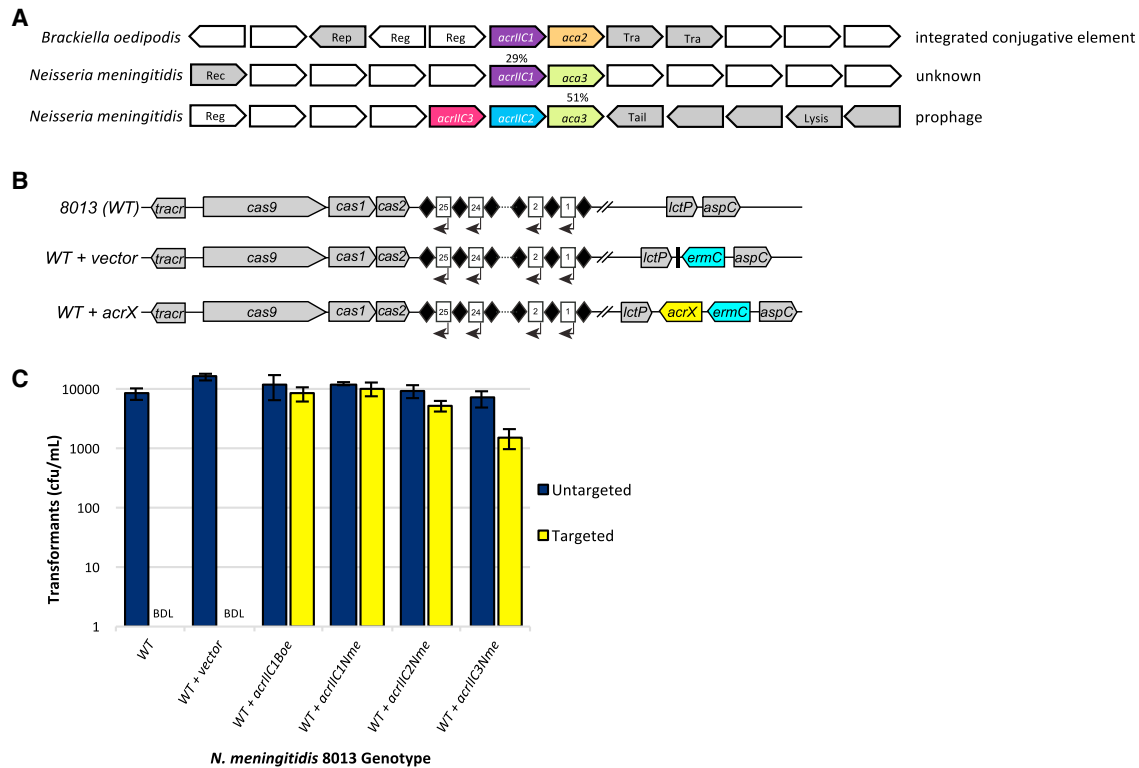


Figure 1. Identification and Validation of Type II-C Anti-CRISPRs

(A) Schematic representation of candidate type II-C *acr* and *aca* genes within putative MGEs in the genomes of strains of *Brackiella oedipodis* and *Neisseria meningitidis*. Homologous genes are color-matched, with percent amino acid identities indicated. Gene arrows are not drawn to scale. Any known, relevant gene product functions are annotated as follows: Rep, plasmid replication protein; Reg, transcriptional regulator; Tra, conjugal transfer protein; Rec, recombinase; Tail, phage tail structural protein; Lysis, phage lysis cassette. Genes colored in gray have MGE-related functions and/or show clear evidence of horizontal transfer. (B) Schematic representation of genotypes in *N. meningitidis* strains used to test candidate anti-CRISPR function. Diamonds, CRISPR repeats; numbered rectangles, CRISPR spacers; arrows, CRISPR transcription. *ermC*, integrated erythromycin resistance cassette; *acrX*, integrated candidate anti-CRISPR cassette. Individual genetic elements are not to scale.

(C) Candidate type II-C anti-CRISPRs inhibit CRISPR interference in *N. meningitidis*. Results of the transformation assay in *N. meningitidis* strain 8013 and isogenic derivatives with each indicated *acr* gene integrated at the *nics* locus (see B) are plotted. The CRISPR-targeted protospacer plasmid (yellow) cannot transform wild-type and empty vector-containing cells due to an active CRISPR-Cas system, resulting in zero transformants. BDL, below detection limit of this assay. Plasmid DNA that lacks a target protospacer sequence can transform all strains equally well (navy). Experiments were repeated three times and error bars represent the standard error of the mean (SEM) between three replicates. Cells were also plated on non-selective media and the total number of cfu/mL present was equivalent in each sample (data not shown).

See also Figure S1 and Tables S1 and S2.

assay described above, we showed that both of these genes displayed robust anti-CRISPR activity (Figures 1B and 1C), and we named them *acrIIC2*_{Nme} and *acrIIC3*_{Nme} (Tables S1 and S2). Based on this result, we classified the HTH protein-coding gene as a bona fide *aca* gene, making it the third such family, hereafter referred to as *aca3*. Overall, these results demonstrate the existence of three distinct families of anti-CRISPR genes that are active against a type II CRISPR-Cas system.

Type II-C Anti-CRISPR Proteins Interact Directly with NmeCas9 to Prevent DNA Cleavage

To determine whether the type II-C anti-CRISPRs function by directly interacting with NmeCas9, we mixed purified, untagged anti-CRISPR proteins with purified, 6xHis-tagged NmeCas9 protein (preloaded with coexpressed sgRNA) and conducted nickel affinity chromatography to assess whether the anti-CRISPRs

directly bound NmeCas9 in vitro. We found that *AcrIIC1*_{Nme}, *AcrIIC2*_{Nme}, and *AcrIIC3*_{Nme} were all retained on the nickel column, reflecting association with NmeCas9. By contrast, a previously identified type I anti-CRISPR protein (*AcrE2*) (Pawluk et al., 2014) did not associate with NmeCas9 (Figures 2A and S2). In a parallel experiment, the anti-CRISPRs did not bind significantly to AnaCas9 (Figures 2B and S2) (Jinek et al., 2014; Ma et al., 2015a), a distantly related type II-C Cas9 homolog with ~20% sequence identity to NmeCas9. These data demonstrate that the anti-CRISPRs identified in this study specifically bind to NmeCas9.

To assess the effect of the anti-CRISPRs on Cas9 enzymatic activity, in vitro DNA cleavage assays were performed. When purified NmeCas9 was loaded with in vitro transcribed single-guide RNA (sgRNA) and then mixed with target DNA, robust and specific cleavage was observed (Figure 3), as described previously

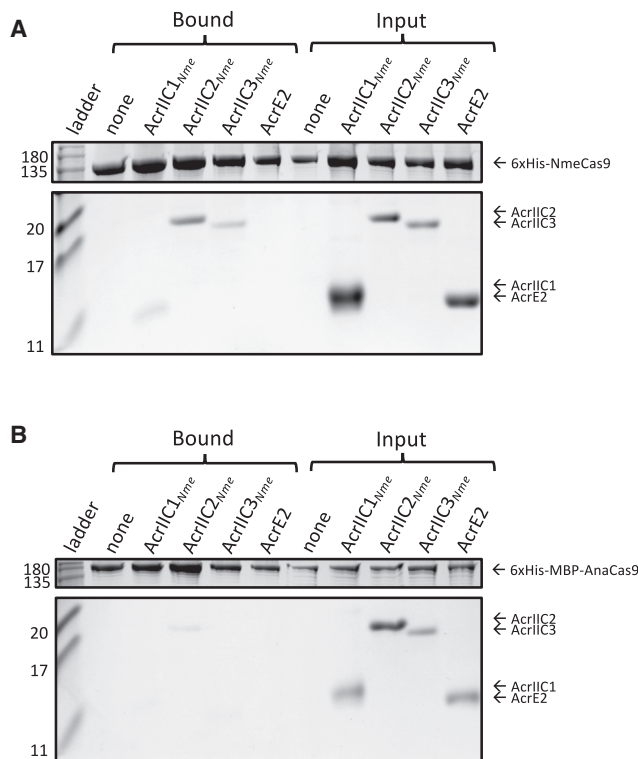


Figure 2. Anti-CRISPRs Bind Directly to NmeCas9:sgRNA
 (A) Purified, untagged anti-CRISPR proteins were mixed with purified, 6xHis tagged NmeCas9:sgRNA in vitro. The input and elution fractions (before and after nickel affinity purification) are shown on the right and left sides of the Coomassie-stained SDS-PAGE gel, respectively. Mobility of marker proteins (in kDa) are denoted on the left. AcrE2 is an inhibitor of the type I-E CRISPR-Cas system and is included in this assay as a negative control. The gel image was cropped to conserve space and to remove irrelevant bands resulting from Cas9 degradation. The image is representative of at least three replicates. Uncropped gel images are presented in [Figure S2](#).
 (B) Binding assays were carried out between the same anti-CRISPRs tested in (A) and Cas9 from *Actinomyces naeslundii* (AnaCas9). AnaCas9 is a distantly related type II-C Cas9 protein (~20% amino acid sequence identity with NmeCas9). The image is representative of at least three replicates.

([Zhang et al., 2015](#)). Cleavage was unaffected by prior incubation of NmeCas9 with increasing amounts of the control, type I-specific anti-CRISPR, AcrE2. In contrast, addition of the *N. meningitidis* anti-CRISPRs to these reactions resulted in inhibition of NmeCas9-catalyzed cleavage in a dose-dependent manner. ~50% cleavage inhibition resulted when the anti-CRISPRs were added at a 1:1 molar ratio, and complete inhibition was seen at a 5:1 anti-CRISPR:NmeCas9 ratio ([Figure 3](#)). The DNA cleavage activity of *S. pyogenes* Cas9 (SpyCas9), which is the most commonly used Cas9 for genome editing, was not affected by addition of any of the anti-CRISPRs ([Figure 3](#), lower panel). This result was expected because SpyCas9 belongs to the type II-A CRISPR-Cas subtype and is very distantly related to NmeCas9. Overall, these in vitro data clearly demonstrate that these anti-CRISPRs directly bind to and specifically inhibit the DNA cleavage activity of NmeCas9. The inhibitory effects of anti-CRISPRs on NmeCas9 in its sgRNA-loaded form

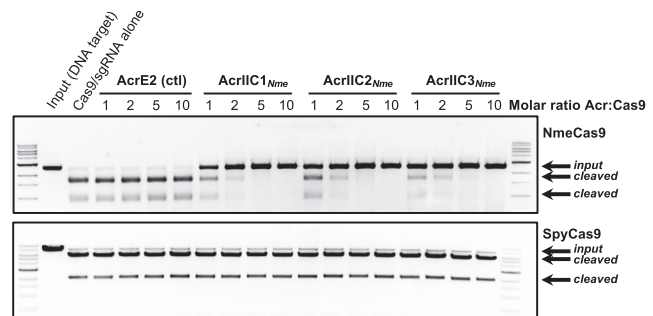


Figure 3. Type II-C Anti-CRISPRs Specifically Block DNA Cleavage by NmeCas9 In Vitro
 Linearized plasmid DNA bearing a protospacer adjacent to a PAM sequence was subjected to in vitro digestion by purified, recombinant, sgRNA-programmed NmeCas9 (upper panel) or SpyCas9 (lower panel). Where indicated at the top of each lane, Cas9 was pre-incubated with purified anti-CRISPR proteins as indicated with AcrE2 as a negative control. Molar equivalents of anti-CRISPR protein (relative to Cas9) are shown at the top of each lane, and mobility of input and cleaved DNAs are denoted on the right. The NmeCas9 cleavage assays shown are representative of three independent replicates.

imply that the natural protective functions of the anti-CRISPR proteins require inhibition of CRISPR RNA (crRNA)/trans-activating crRNA (tracrRNA)-loaded NmeCas9 that is already present in the host cell at the time of phage infection.

Anti-CRISPRs Inhibit Genome Editing by NmeCas9 in Cultured Human Cells

Our discovery of direct inhibitors of NmeCas9 activity raised the possibility that these anti-CRISPRs could be used as off-switches for CRISPR-Cas9 genome editing in mammalian cells. To address this, we co-transfected HEK293T cells with three plasmids: one expressing Cas9, one expressing a genome-targeting sgRNA, and one expressing an anti-CRISPR. Genome editing efficiency was determined using an established T7 endonuclease 1 (T7E1)-based protocol. Strikingly, we found that each of the anti-CRISPRs greatly decreased the ability of NmeCas9 to create genome lesions in cultured human cells ([Figures 4, S3, and S4; Table S3](#)). Because the anti-CRISPRs are all below ~14 kDa (i.e., small enough to diffuse freely through nuclear pores), they inhibited NmeCas9 genome editing even without an appended, heterologous nuclear localization sequence (NLS). Plasmid titration experiments demonstrated that the three anti-CRISPR families could each completely inhibit editing, with AcrIIC3_{Nme} appearing to be the most potent ([Figure S4](#)). The superior potency of AcrIIC3_{Nme} anti-CRISPR activity in mammalian cells is noteworthy given that it was slightly less effective at inhibiting transformation interference in meningococcal cells ([Figure 1C](#)). The variations in activities of these anti-CRISPRs in mammalian cells are likely due to differences in expression or stability as they all displayed similar inhibitory activities in vitro ([Figure 3](#)). Consistent with our in vitro results, the anti-CRISPRs had no effect on editing mediated by SpyCas9 targeting the same genomic site ([Figures 4 and S3](#)). In addition, type I-E anti-CRISPR AcrE2 had no significant inhibitory effect in any of these experiments. In no instance did we observe any sign of cellular toxicity by any anti-CRISPR. In summary, these human

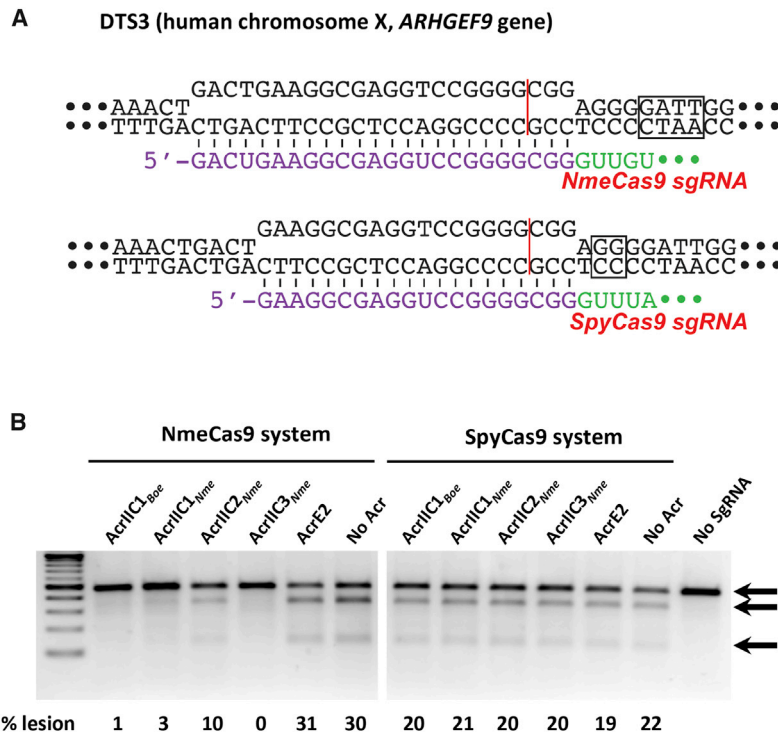


Figure 4. Type II-C Anti-CRISPRs Specifically Block Genome Editing by NmeCas9 in Human Cells

(A) Schematic representation of R-loop structures at a dual target site (DTS3) in the human genome that can be cleaved and edited by either SpyCas9 (top) or NmeCas9 (bottom). Guide sequences (purple), PAMs (boxed), and Cas9 cleavage sites (red line) are indicated.

(B) T7E1 assays of NmeCas9 or SpyCas9 editing efficiencies at DTS3 upon transient transfection of human HEK293T cells. Constructs encoding anti-CRISPR proteins were co-transfected as indicated at the top of each lane. Mobility of T7E1-digested (edited) and -undigested (unedited) bands are indicated to the right, and editing efficiencies (“% lesion”) are given at the bottom of each lane. These images are representative of at least seven replicates. See also Figures S3 and S4 and Table S3.

cell experiments illustrate the potential application of these anti-CRISPRs for precise control of Cas9-mediated genome editing.

AcrIIIC3_{Nme} Prevents dNmeCas9 Genome Binding in Cultured Human Cells

“Dead” Cas9 (dCas9) orthologs, including dNmeCas9 (Esvelt et al., 2013; Hilton et al., 2015; Kearns et al., 2015; Ma et al., 2015b), have proven to be exceptionally useful for RNA-guided DNA binding (without Cas9-catalyzed DNA cleavage), because a wide range of domains and functionalities can be fused or tethered to the DNA-bound dCas9/sgrNA complex (Dominguez et al., 2016; Wang et al., 2016). In principle, anti-CRISPR inhibition of sgRNA-guided NmeCas9 DNA cleavage (Figure 3) and genome editing (Figure 4) could reflect either inhibition upstream of stable R-loop formation, or inhibition of NmeCas9 catalytic activation after stable R-loop formation. In the former case, the anti-CRISPR could be used as an off-switch not only for genome editing, but also for dNmeCas9 DNA binding applications such as CRISPRi and CRISPRa (Dominguez et al., 2016; Wang et al., 2016). To determine whether our most potent genome editing inhibitor (AcrIIIC3_{Nme}) can prevent stable DNA binding by dNmeCas9 in mammalian cells, we used a previously developed system in which superfolder (sf) GFP-labeled dNmeCas9 and mCherry-labeled dSpyCas9 are simultaneously colocalized to telomeric loci by cognate sgRNAs upon co-transfection of their expression plasmids in U2OS cells (Ma et al., 2015b) (Figure 5A). We readily observed colocalizing telomeric dNmeCas9-(sfGFP)₃ and dSpyCas9-(mCherry)₃ foci as long as both of the telomere-directed sgRNAs were included for the two dCas9 orthologs (Figures 5B–5D), as reported previously (Ma et al., 2015b). We then repeated the experiment with the co-transfected, mTagBFP2-

marked plasmid (Figure 5A, bottom) also carrying an anti-CRISPR expression cassette. AcrE2 had no effect on telomeric co-localization of dNmeCas9-(sfGFP)₃ and dSpyCas9-(mCherry)₃, as expected (Figure 5E). In contrast, co-expression of AcrIIIC3_{Nme} prevented the co-localization of dNmeCas9-(sfGFP)₃ with the dSpyCas9-(mCherry)₃ telomeric foci (Figure 5F). We then repeated this experiment in a blinded fashion, with unidentified samples that had been coded by a separate experimenter. Only cells that exhibited mTagBFP2 and sfGFP fluorescence as well as dSpyCas9-(mCherry)₃ telomeric foci were assessed for the presence or absence of co-localizing dNmeCas9-(sfGFP)₃ telomeric foci, and all such imaged cells were included in our quantifications. The results were tabulated, decoded, and plotted as a bar graph (Figure 5G). Telomeric dNmeCas9-(sfGFP)₃ foci were observed in 94% (31 out of 33) of cells in the absence of any Acr protein and 88% (31 out of 37) of cells in the presence of the negative control AcrE2 protein. By contrast, 0% of cells (0 out of 46) exhibited dNmeCas9-(sfGFP)₃ telomeric foci when AcrIIIC3_{Nme} was coexpressed. These results confirm the robust inhibitory effect of AcrIIIC3_{Nme} on stable, sgRNA-programmed DNA binding by dNmeCas9 and indicate that it can be used as a potent off-switch not only for NmeCas9 genome editing, but also for dNmeCas9-based applications in mammalian cells.

A Wide Range of Type II-C CRISPR-Cas Systems Are Likely Susceptible to Inhibition by Anti-CRISPRs

CRISPR-Cas systems are divided into two broad classes, each encompassing several types and many subtypes. Class 1 systems employ multi-subunit surveillance complexes, whereas class 2 systems have single, large effector proteins like Cas9 (Markarova et al., 2015). Our previous studies on anti-CRISPRs acting on type I systems (belonging to Class 1) suggest that each anti-CRISPR protein acts on a particular range of systems within one subtype due to the specificity of protein-protein interactions between the anti-CRISPR and Cas proteins (Bondy-Denomy

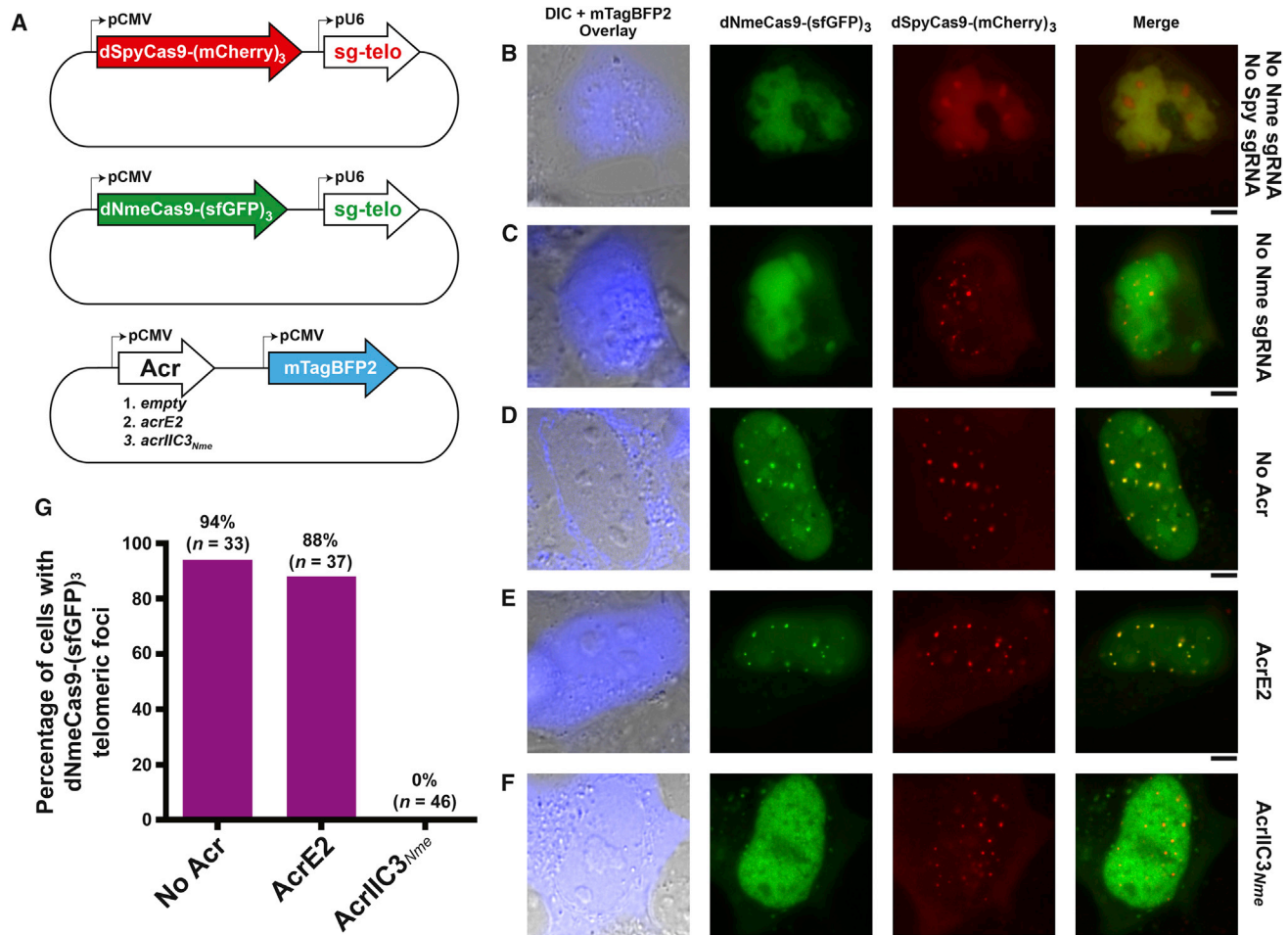


Figure 5. AcrIIC3_{Nme} Prevents DNA Binding by NmeCas9 in Human Cells

(A) Schematic representation of plasmids used for expression of dNmeCas9-(sfGFP)₃, dSpyCas9-(mCherry)₃, their respective telomeric sgRNAs, and anti-CRISPR protein. The plasmid encoding the anti-CRISPR protein is also marked with the blue fluorescent protein mTagBFP2.

(B–F) Fluorescence images of U2OS cells transiently transfected with plasmids depicted in (A). The specific version of each plasmid set (with or without sgRNAs, with or without anti-CRISPRs) is given to the right of each row. First column: differential interference contrast (DIC) and mTagBFP2 imaging, merged. Second column: dNmeCas9-(sfGFP)₃. Third column: dSpyCas9-(mCherry)₃. Fourth column: dNmeCas9-(sfGFP)₃ and dSpyCas9-(mCherry)₃, merged. (B) No sgRNAs for either dNmeCas9-(sfGFP)₃ or dSpyCas9-(mCherry)₃. (C) No sgRNA for dNmeCas9-(sfGFP)₃. (D) No Acr protein. (E) With AcrE2 (negative control anti-CRISPR). (F) With AcrIIC3_{Nme}. Scale bars, 5 μm.

(G) Quantitation of dNmeCas9-(sfGFP)₃ telomeric foci, as judged by co-localization with dSpyCas9-(mCherry)₃ telomeric foci, in cells that express no anti-CRISPR, negative control anti-CRISPR (AcrE2), or AcrIIC3_{Nme}. Foci were scored blind, i.e., without the experimenter knowing the sample identities (see STAR Methods). n = number of cells that were scored in each condition.

et al., 2013, 2015; Pawluk et al., 2014, 2016). An anti-CRISPR gene will likely be selected for if it inhibits the CRISPR-Cas system of the bacterium in which it is found, as these genes are almost always located on MGEs that have successfully invaded a host. This principle was used to accurately predict that the anti-CRISPRs described here would block the type II-C CRISPR-Cas system of *N. meningitidis*.

To visualize the potential general impact of anti-CRISPR activity on type II CRISPR-Cas systems, we created a phylogenetic tree of Cas9, which is the sole effector protein of these systems and the direct binding target of the type II-C anti-CRISPRs (Figure 6). Bacterial genera in which known type II-C anti-CRISPR homologs are encoded are indicated in red.

From this analysis, based on the phylogenetic breadth spanned by the anti-CRISPR putative orthologs, we propose that the majority of type II-C CRISPR-Cas diversity may be susceptible to at least one member of an anti-CRISPR family discovered in this study. These data, combined with our previous analysis of type I-F CRISPR-Cas systems and their cognate anti-CRISPRs, suggests that even the relatively small number of anti-CRISPR gene families discovered to date have a broad impact on CRISPR-Cas systems in bacteria. Now that anti-CRISPRs inhibiting both Class 1 and class 2 CRISPR-Cas systems have been described, we expect that anti-CRISPRs able to inhibit all types and subtypes of CRISPR-Cas systems exist and await discovery.

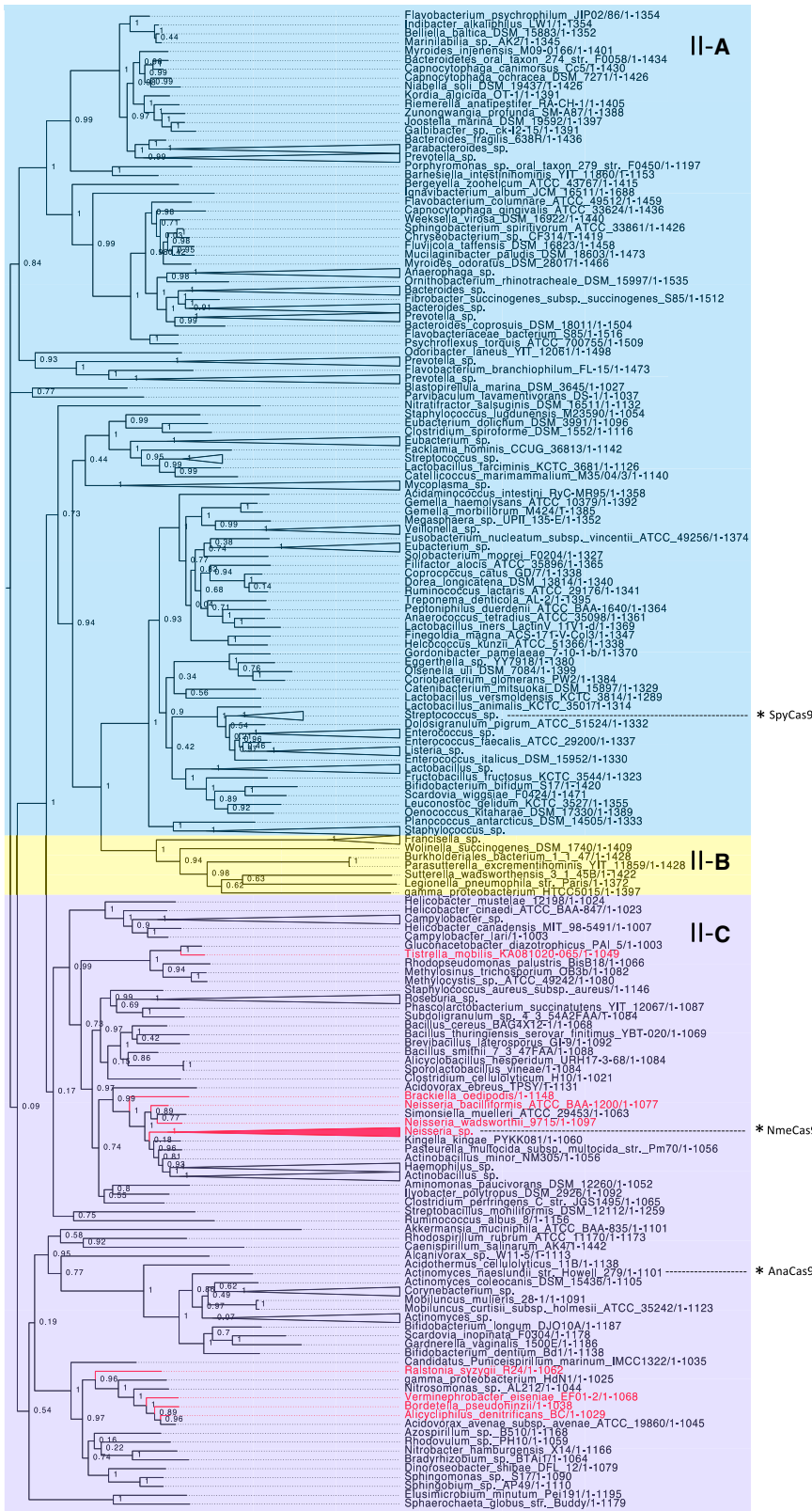


Figure 6. Anti-CRISPRs Likely Have a Broad Impact on Diverse CRISPR-Cas Systems

A maximum likelihood phylogenetic tree of representative Cas9 protein sequences. Each protein is classified based on the CRISPR locus in which it resides as type II-A (blue), type II-B (yellow), or type II-C (purple). Cas9 proteins belonging to any genus that has a type II-C anti-CRISPR putative ortholog are colored in red. With the assumption that a given anti-CRISPR ortholog inhibits the CRISPR-Cas system in the species where it is found, this visualization provides an estimate of the breadth of activity encompassed by the anti-CRISPR families discovered here. The position of notable Cas9 orthologs on the tree are indicated by asterisks.

DISCUSSION

In this work, we report that protein inhibitors of CRISPR interference, previously reported only for type I CRISPR-Cas systems, now extend into the type II systems that employ Cas9. Importantly, we show that the three different families of type II-C anti-CRISPRs that we have identified can be used to block genome editing by NmeCas9 in cultured human cells. Genetically encoded Cas9 inhibitors provide a means to spatially, temporally, or conditionally control Cas9 activity, thereby potentially allowing tissue-, cell-cycle stage-, developmental stage-, or stimulus-specific inactivation of genome editing. Target site precision and tissue specificity are important safety concerns when considering CRISPR-Cas9 applications in gene therapy, and prolonged or misexpressed nuclease activity may exacerbate undesirable off-target effects. Effective Cas9 off-switches could ameliorate this difficulty through expression or delivery strategies that would enable anti-CRISPR proteins to accumulate whenever or wherever editing activity is unwanted. Finally, for gene drive applications employing CRISPR-Cas9 to force inheritance of desired alleles (e.g., in insect populations), possession of a functioning off-switch may provide a useful security or containment measure to avert unintended adverse consequences.

We have shown that members of all three anti-CRISPR families studied here bind directly to the NmeCas9/sgRNA complex and inhibit *in vitro* DNA cleavage. Given the completely unrelated sequences of these anti-CRISPRs, we expect that they may abrogate activity through different mechanisms, as was the case for three type I-F anti-CRISPRs previously characterized in our laboratory (Bondy-Denomy et al., 2015). We have already determined that AcrIIIC3_{Nme} prevents stable genomic localization of sgRNA-loaded dNmeCas9 in mammalian cells, indicating that it could be used as an off-switch for dNmeCas9-based applications. It remains possible that other anti-CRISPRs allow NmeCas9 DNA-binding activity but prevent catalytic activation. If so, this would effectively create an NmeCas9 complex with utility for modulation of transcription (Dominguez et al., 2016; Wang et al., 2016). We have identified a type I-F anti-CRISPR possessing this property (Bondy-Denomy et al., 2015).

Apart from their potential for biotechnological applications, the evolutionary implications of anti-CRISPRs are profound. CRISPR-Cas systems are present in approximately half of sequenced prokaryotic genomes and are widespread across diverse bacterial and archaeal lineages. The extreme diversity in and purifying selective pressure on CRISPR-Cas systems, combined with the co-occurrence of several different CRISPR-Cas system types in many genomes, is indicative of a dynamic co-evolutionary battle for survival between prokaryotes and parasitic MGEs (Makarova et al., 2015; Takeuchi et al., 2012). CRISPR-Cas systems are expected to pose a significant challenge to the process of horizontal gene transfer, especially given their ability to acquire heritable immunity against newly encountered threats and to upgrade their arsenal through new spacer acquisition (Barrangou et al., 2007; Fineran et al., 2014; Richter et al., 2014). However, recent studies have shown that the presence of a CRISPR-Cas system does not correlate with lower

levels of horizontal gene transfer (HGT) over evolutionary time-scales, or with a lower number of acquired prophage elements (Gophna et al., 2015; Touchon et al., 2016). We propose that widespread MGE-encoded anti-CRISPRs could reconcile this paradox. Also from an evolutionary perspective, we note that Cas9 from type II-A systems is essential not only for the interference function of existing spacers, but also for the adaptive acquisition of new spacers (Heler et al., 2015; Wei et al., 2015). If this adaptation role of type II-A Cas9 extends to type II-C systems, as seems likely, then Cas9-associating anti-CRISPRs may prevent the acquisition of new spacers in response to ongoing invasions.

A recent *in vitro* evolution study showed that the only way for phages to escape CRISPR-mediated extinction is by the expression of an anti-CRISPR gene (van Houte et al., 2016). In strong accordance with the Red Queen theory, we have discovered a total of seventeen distinct anti-CRISPR protein families that are widespread among Proteobacteria, each inhibiting either type I-E, I-F, or II-C systems (Bondy-Denomy et al., 2013; Pawluk et al., 2014; Pawluk et al., 2016). The fact that anti-CRISPRs have evolved to inhibit both Class 1 and class 2 CRISPR-Cas systems strongly suggests that they exist for other CRISPR-Cas types as well. We anticipate that anti-CRISPR activity has a large impact on CRISPR-Cas systems across prokaryotes and a profound effect on horizontal gene transfer.

STAR★METHODS

Detailed methods are provided in the online version of this paper and include the following:

- KEY RESOURCES TABLE
- CONTACT FOR REAGENT AND RESOURCE SHARING
- EXPERIMENTAL MODEL AND SUBJECT DETAILS
 - *Neisseria meningitidis* strain 8013
 - *Escherichia coli* Rosetta (DE3)
 - *Escherichia coli* BL21 (DE3)
 - HEK293T
 - U2OS
- METHOD DETAILS
 - Bioinformatics analysis
 - Plasmid Construction
 - *Neisseria meningitidis* natural transformation
 - Cloning and purification of anti-CRISPR proteins
 - Purification of Cas9
 - Cas9-anti-CRISPR pulldown assays
 - *In vitro* DNA cleavage
 - Mammalian genome editing
 - Fluorescence microscopy of dNmeCas9
- QUANTIFICATION AND STATISTICAL ANALYSIS
 - *Neisseria meningitidis* transformation efficiency
 - Genome editing efficiency
 - Fluorescence imaging

SUPPLEMENTAL INFORMATION

Supplemental Information includes four figures and three tables and can be found with this article online at <http://dx.doi.org/10.1016/j.cell.2016.11.017>.

AUTHOR CONTRIBUTIONS

A.P. conducted bioinformatics analysis, designed experiments, purified proteins, performed Cas9-anti-CRISPR interaction experiments, and wrote the manuscript. N.A. designed and performed human genome-editing experiments. Y.Z. designed and performed *N. meningitidis* transformation experiments. B.G. and Y.H.-R. purified proteins and performed Cas9-anti-CRISPR interaction experiments. J.L. performed fluorescence live-cell-imaging experiments. A.E. purified NmeCas9 and conducted in vitro DNA cleavage experiments. M.S. assisted in anti-CRISPR and NmeCas9 protein purification. E.J.S., K.L.M., and A.R.D. supervised experimental work and wrote the manuscript.

ACKNOWLEDGMENTS

The authors would like to thank Sabrina Stanley for technical assistance. The AnaCas9 expression construct was a generous gift from Lucas Harrington, Enbo Ma, and Jennifer Doudna. We are grateful to David Grünwald and members of his lab for help and advice with fluorescence imaging and to Andrew Franck for help and advice with NmeCas9 purification. We thank Scot Wolfe and Wen Xue for helpful discussions and comments on the manuscript. This work was supported by a Canadian Institutes of Health Research Doctoral Award to A.P., NIH grant K99 GM117268 to Y.Z., NIH grant R01 GM115911 to E.J.S., and Canadian Institutes of Health Research grants to A.R.D. (MOP-130482) and K.L.M. (MOP-136845). E.J.S. is a co-founder and scientific advisor of Intellia Therapeutics. The authors have filed for a patent related to this work.

Received: October 5, 2016

Revised: November 7, 2016

Accepted: November 9, 2016

Published: December 8, 2016

REFERENCES

Barrangou, R., Fremaux, C., Deveau, H., Richards, M., Boyaval, P., Moineau, S., Romero, D.A., and Horvath, P. (2007). CRISPR provides acquired resistance against viruses in prokaryotes. *Science* 315, 1709–1712.

Bikard, D., Euler, C.W., Jiang, W., Nussenzweig, P.M., Goldberg, G.W., Duportet, X., Fischetti, V.A., and Marraffini, L.A. (2014). Exploiting CRISPR-Cas nucleases to produce sequence-specific antimicrobials. *Nat. Biotechnol.* 32, 1146–1150.

Bolukbasi, M.F., Gupta, A., and Wolfe, S.A. (2016). Creating and evaluating accurate CRISPR-Cas9 scalpels for genomic surgery. *Nat. Methods* 13, 41–50.

Bondy-Denomy, J., Pawluk, A., Maxwell, K.L., and Davidson, A.R. (2013). Bacteriophage genes that inactivate the CRISPR/Cas bacterial immune system. *Nature* 493, 429–432.

Bondy-Denomy, J., Garcia, B., Strum, S., Du, M., Rollins, M.F., Hidalgo-Reyes, Y., Wiedenheft, B., Maxwell, K.L., and Davidson, A.R. (2015). Multiple mechanisms for CRISPR-Cas inhibition by anti-CRISPR proteins. *Nature* 526, 136–139.

Cho, S.W., Kim, S., Kim, J.M., and Kim, J.S. (2013). Targeted genome engineering in human cells with the Cas9 RNA-guided endonuclease. *Nat. Biotechnol.* 31, 230–232.

Cong, L., Ran, F.A., Cox, D., Lin, S., Barretto, R., Habib, N., Hsu, P.D., Wu, X., Jiang, W., Marraffini, L.A., and Zhang, F. (2013). Multiplex genome engineering using CRISPR/Cas systems. *Science* 339, 819–823.

Deltcheva, E., Chylinski, K., Sharma, C.M., Gonzales, K., Chao, Y., Pirzada, Z.A., Eckert, M.R., Vogel, J., and Charpentier, E. (2011). CRISPR RNA maturation by trans-encoded small RNA and host factor RNase III. *Nature* 471, 602–607.

Dominguez, A.A., Lim, W.A., and Qi, L.S. (2016). Beyond editing: repurposing CRISPR-Cas9 for precision genome regulation and interrogation. *Nat. Rev. Mol. Cell Biol.* 17, 5–15.

Duffin, P.M., and Seifert, H.S. (2012). Genetic transformation of *Neisseria gonorrhoeae* shows a strand preference. *FEMS Microbiol. Lett.* 334, 44–48.

Ebina, H., Misawa, N., Kanemura, Y., and Koyanagi, Y. (2013). Harnessing the CRISPR/Cas9 system to disrupt latent HIV-1 provirus. *Sci. Rep.* 3, 2510.

Edgar, R.C. (2004). MUSCLE: multiple sequence alignment with high accuracy and high throughput. *Nucleic Acids Res.* 32, 1792–1797.

Esvelt, K.M., Mali, P., Braff, J.L., Moosburner, M., Yaung, S.J., and Church, G.M. (2013). Orthogonal Cas9 proteins for RNA-guided gene regulation and editing. *Nat. Methods* 10, 1116–1121.

Fineran, P.C., Gerritzen, M.J., Suárez-Diez, M., Künne, T., Boekhorst, J., van Hijum, S.A., Staals, R.H., and Brouns, S.J. (2014). Degenerate target sites mediate rapid primed CRISPR adaptation. *Proc. Natl. Acad. Sci. USA* 111, E1629–E1638.

Fonfara, I., Le Rhun, A., Chylinski, K., Makarova, K.S., Lécrivain, A.L., Bzdrenga, J., Koonin, E.V., and Charpentier, E. (2014). Phylogeny of Cas9 determines functional exchangeability of dual-RNA and Cas9 among orthologous type II CRISPR-Cas systems. *Nucleic Acids Res.* 42, 2577–2590.

Fu, Y., Sander, J.D., Reyon, D., Cascio, V.M., and Joung, J.K. (2014). Improving CRISPR-Cas nuclease specificity using truncated guide RNAs. *Nat. Biotechnol.* 32, 279–284.

Gantz, V.M., Jasinskiene, N., Tatarenkova, O., Fazekas, A., Macias, V.M., Bier, E., and James, A.A. (2015). Highly efficient Cas9-mediated gene drive for population modification of the malaria vector mosquito *Anopheles stephensi*. *Proc. Natl. Acad. Sci. USA* 112, E6736–E6743.

Gasiunas, G., Barrangou, R., Horvath, P., and Siksnys, V. (2012). Cas9-crRNA ribonucleoprotein complex mediates specific DNA cleavage for adaptive immunity in bacteria. *Proc. Natl. Acad. Sci. USA* 109, E2579–E2586.

Gomaa, A.A., Klumpe, H.E., Luo, M.L., Selle, K., Barrangou, R., and Beisel, C.L. (2014). Programmable removal of bacterial strains by use of genome-targeting CRISPR-Cas systems. *MBio* 5, e00928–13.

Gophna, U., Kristensen, D.M., Wolf, Y.I., Popa, O., Drevet, C., and Koonin, E.V. (2015). No evidence of inhibition of horizontal gene transfer by CRISPR-Cas on evolutionary timescales. *ISME J.* 9, 2021–2027.

Guschin, D.Y., Waite, A.J., Katibah, G.E., Miller, J.C., Holmes, M.C., and Rebar, E.J. (2010). A rapid and general assay for monitoring endogenous gene modification. *Methods Mol. Biol.* 649, 247–256.

Hammond, A., Galizi, R., Kyrou, K., Simoni, A., Siniscalchi, C., Katsanos, D., Gribble, M., Baker, D., Marois, E., Russell, S., et al. (2016). A CRISPR-Cas9 gene drive system targeting female reproduction in the malaria mosquito vector *Anopheles gambiae*. *Nat. Biotechnol.* 34, 78–83.

Heler, R., Samai, P., Modell, J.W., Weiner, C., Goldberg, G.W., Bikard, D., and Marraffini, L.A. (2015). Cas9 specifies functional viral targets during CRISPR-Cas adaptation. *Nature* 519, 199–202.

Hilton, I.B., D'Ippolito, A.M., Vockley, C.M., Thakore, P.I., Crawford, G.E., Reddy, T.E., and Gersbach, C.A. (2015). Epigenome editing by a CRISPR-Cas9-based acetyltransferase activates genes from promoters and enhancers. *Nat. Biotechnol.* 33, 510–517.

Hirano, H., Gootenberg, J.S., Horii, T., Abudayyeh, O.O., Kimura, M., Hsu, P.D., Nakane, T., Ishitani, R., Hatada, I., Zhang, F., et al. (2016). Structure and engineering of *Francisella novicida* Cas9. *Cell* 164, 950–961.

Hou, Z., Zhang, Y., Propson, N.E., Howden, S.E., Chu, L.F., Sontheimer, E.J., and Thomson, J.A. (2013). Efficient genome engineering in human pluripotent stem cells using Cas9 from *Neisseria meningitidis*. *Proc. Natl. Acad. Sci. USA* 110, 15644–15649.

Hsu, P.D., Scott, D.A., Weinstein, J.A., Ran, F.A., Konermann, S., Agarwala, V., Li, Y., Fine, E.J., Wu, X., Shalem, O., et al. (2013). DNA targeting specificity of RNA-guided Cas9 nucleases. *Nat. Biotechnol.* 31, 827–832.

Hwang, W.Y., Fu, Y., Reyon, D., Maeder, M.L., Kaini, P., Sander, J.D., Joung, J.K., Peterson, R.T., and Yeh, J.R. (2013). Heritable and precise zebrafish genome editing using a CRISPR-Cas system. *PLoS ONE* 8, e68708.

Jiang, W., Bikard, D., Cox, D., Zhang, F., and Marraffini, L.A. (2013). RNA-guided editing of bacterial genomes using CRISPR-Cas systems. *Nat. Biotechnol.* 31, 233–239.

- Jinek, M., Chylinski, K., Fonfara, I., Hauer, M., Doudna, J.A., and Charpentier, E. (2012). A programmable dual-RNA-guided DNA endonuclease in adaptive bacterial immunity. *Science* 337, 816–821.
- Jinek, M., East, A., Cheng, A., Lin, S., Ma, E., and Doudna, J. (2013). RNA-programmed genome editing in human cells. *eLife* 2, e00471.
- Jinek, M., Jiang, F., Taylor, D.W., Sternberg, S.H., Kaya, E., Ma, E., Anders, C., Hauer, M., Zhou, K., Lin, S., et al. (2014). Structures of Cas9 endonucleases reveal RNA-mediated conformational activation. *Science* 343, 1247997.
- Kaminski, R., Chen, Y., Fischer, T., Tedaldi, E., Napoli, A., Zhang, Y., Karn, J., Hu, W., and Khalili, K. (2016). Elimination of HIV-1 genomes from human t-lymphoid cells by CRISPR/Cas9 Gene Editing. *Sci. Rep.* 6, 22555.
- Kearns, N.A., Genga, R.M., Enuameh, M.S., Garber, M., Wolfe, S.A., and Maehr, R. (2014). Cas9 effector-mediated regulation of transcription and differentiation in human pluripotent stem cells. *Development* 141, 219–223.
- Kearns, N.A., Pham, H., Tabak, B., Genga, R.M., Silverstein, N.J., Garber, M., and Maehr, R. (2015). Functional annotation of native enhancers with a Cas9-histone demethylase fusion. *Nat. Methods* 12, 401–403.
- Lee, C.M., Cradick, T.J., and Bao, G. (2016). The *Neisseria meningitidis* CRISPR-Cas9 System Enables Specific Genome Editing in Mammalian Cells. *Mol. Ther.* 24, 645–654.
- Ma, E., Harrington, L.B., O’Connell, M.R., Zhou, K., and Doudna, J.A. (2015a). Single-stranded DNA cleavage by divergent CRISPR-Cas9 enzymes. *Mol. Cell* 60, 398–407.
- Ma, H., Naseri, A., Reyes-Gutierrez, P., Wolfe, S.A., Zhang, S., and Pederson, T. (2015b). Multicolor CRISPR labeling of chromosomal loci in human cells. *Proc. Natl. Acad. Sci. USA* 112, 3002–3007.
- Makarova, K.S., Wolf, Y.I., Alkhnbashi, O.S., Costa, F., Shah, S.A., Saunders, S.J., Barrangou, R., Brouns, S.J., Charpentier, E., Haft, D.H., et al. (2015). An updated evolutionary classification of CRISPR-Cas systems. *Nat. Rev. Microbiol.* 13, 722–736.
- Mali, P., Yang, L., Esvelt, K.M., Aach, J., Guell, M., DiCarlo, J.E., Norville, J.E., and Church, G.M. (2013). RNA-guided human genome engineering via Cas9. *Science* 339, 823–826.
- Müller, M., Lee, C.M., Gasiunas, G., Davis, T.H., Cradick, T.J., Siksnys, V., Bao, G., Cathomen, T., and Mussolino, C. (2016). *Streptococcus thermophilus* CRISPR-Cas9 systems enable specific editing of the human genome. *Mol. Ther.* 24, 636–644.
- Nihongaki, Y., Kawano, F., Nakajima, T., and Sato, M. (2015). Photoactivatable CRISPR-Cas9 for optogenetic genome editing. *Nat. Biotechnol.* 33, 755–760.
- Núñez, J.K., Harrington, L.B., and Doudna, J.A. (2016). Chemical and biophysical modulation of Cas9 for tunable genome engineering. *ACS Chem. Biol.* 11, 681–688.
- Orthwein, A., Noordermeer, S.M., Wilson, M.D., Landry, S., Enchev, R.I., Sherker, A., Munro, M., Pinder, J., Salsman, J., Dellaire, G., et al. (2015). A mechanism for the suppression of homologous recombination in G1 cells. *Nature* 528, 422–426.
- Ousterout, D.G., Kabadi, A.M., Thakore, P.I., Majoros, W.H., Reddy, T.E., and Gersbach, C.A. (2015). Multiplex CRISPR/Cas9-based genome editing for correction of dystrophin mutations that cause Duchenne muscular dystrophy. *Nat. Commun.* 6, 6244.
- Pattanayak, V., Lin, S., Guilinger, J.P., Ma, E., Doudna, J.A., and Liu, D.R. (2013). High-throughput profiling of off-target DNA cleavage reveals RNA-programmed Cas9 nuclease specificity. *Nat. Biotechnol.* 31, 839–843.
- Pawluk, A., Bondy-Denomy, J., Cheung, V.H., Maxwell, K.L., and Davidson, A.R. (2014). A new group of phage anti-CRISPR genes inhibits the type I-E CRISPR-Cas system of *Pseudomonas aeruginosa*. *MBio* 5, e00896.
- Pawluk, A., Staals, R.H.J., Taylor, C., Watson, B.N.J., Saha, S., Fineran, P.C., Maxwell, K.L., and Davidson, A.R. (2016). Inactivation of CRISPR-Cas systems by anti-CRISPR proteins in diverse bacterial species. *Nat. Microbiol.* 1, 16085.
- Peränen, J., Rikkonen, M., Hyvönen, M., and Kääriäinen, L. (1996). T7 vectors with modified T7lac promoter for expression of proteins in *Escherichia coli*. *Anal. Biochem.* 236, 371–373.
- Price, M.N., Dehal, P.S., and Arkin, A.P. (2009). FastTree: computing large minimum evolution trees with profiles instead of a distance matrix. *Mol. Biol. Evol.* 26, 1641–1650.
- Price, M.N., Dehal, P.S., and Arkin, A.P. (2010). FastTree 2—approximately maximum-likelihood trees for large alignments. *PLoS ONE* 5, e9490.
- Ran, F.A., Cong, L., Yan, W.X., Scott, D.A., Gootenberg, J.S., Kriz, A.J., Zetsche, B., Shalem, O., Wu, X., Makarova, K.S., et al. (2015). In vivo genome editing using *Staphylococcus aureus* Cas9. *Nature* 520, 186–191.
- Richter, C., Dy, R.L., McKenzie, R.E., Watson, B.N., Taylor, C., Chang, J.T., McNeil, M.B., Staals, R.H., and Fineran, P.C. (2014). Priming in the Type I-F CRISPR-Cas system triggers strand-independent spacer acquisition, bi-directionally from the primed protospacer. *Nucleic Acids Res.* 42, 8516–8526.
- Takeuchi, N., Wolf, Y.I., Makarova, K.S., and Koonin, E.V. (2012). Nature and intensity of selection pressure on CRISPR-associated genes. *J. Bacteriol.* 194, 1216–1225.
- Touchon, M., Bernheim, A., and Rocha, E.P. (2016). Genetic and life-history traits associated with the distribution of prophages in bacteria. *ISME J.* 10, 2744–2754.
- van Houte, S., Ekroth, A.K., Broniewski, J.M., Chabas, H., Ashby, B., Bondy-Denomy, J., Gandon, S., Boots, M., Paterson, S., Buckling, A., and Westra, E.R. (2016). The diversity-generating benefits of a prokaryotic adaptive immune system. *Nature* 532, 385–388.
- Villefranc, J.A., Amigo, J., and Lawson, N.D. (2007). Gateway compatible vectors for analysis of gene function in the zebrafish. *Dev. Dyn.* 236, 3077–3087.
- Wang, H., Yang, H., Shivalila, C.S., Dawlaty, M.M., Cheng, A.W., Zhang, F., and Jaenisch, R. (2013). One-step generation of mice carrying mutations in multiple genes by CRISPR/Cas-mediated genome engineering. *Cell* 153, 910–918.
- Wang, H., La Russa, M., and Qi, L.S. (2016). CRISPR/Cas9 in genome editing and beyond. *Annu. Rev. Biochem.* 85, 227–264.
- Wei, Y., Terns, R.M., and Terns, M.P. (2015). Cas9 function and host genome sampling in Type II-A CRISPR-Cas adaptation. *Genes Dev.* 29, 356–361.
- Wright, A.V., Sternberg, S.H., Taylor, D.W., Staahl, B.T., Bardales, J.A., Kornfeld, J.E., and Doudna, J.A. (2015). Rational design of a split-Cas9 enzyme complex. *Proc. Natl. Acad. Sci. USA* 112, 2984–2989.
- Wu, Y., Liang, D., Wang, Y., Bai, M., Tang, W., Bao, S., Yan, Z., Li, D., and Li, J. (2013). Correction of a genetic disease in mouse via use of CRISPR-Cas9. *Cell Stem Cell* 13, 659–662.
- Yen, S.T., Zhang, M., Deng, J.M., Usman, S.J., Smith, C.N., Parker-Thornburg, J., Swinton, P.G., Martin, J.F., and Behringer, R.R. (2014). Somatic mosaicism and allele complexity induced by CRISPR/Cas9 RNA injections in mouse zygotes. *Dev. Biol.* 393, 3–9.
- Yin, H., Xue, W., Chen, S., Bogorad, R.L., Benedetti, E., Grompe, M., Kotliansky, V., Sharp, P.A., Jacks, T., and Anderson, D.G. (2014). Genome editing with Cas9 in adult mice corrects a disease mutation and phenotype. *Nat. Biotechnol.* 32, 551–553.
- Zhang, Y., Heidrich, N., Ampattu, B.J., Gunderson, C.W., Seifert, H.S., Schoen, C., Vogel, J., and Sontheimer, E.J. (2013). Processing-independent CRISPR RNAs limit natural transformation in *Neisseria meningitidis*. *Mol. Cell* 50, 488–503.
- Zhang, Y., Rajan, R., Seifert, H.S., Mondragón, A., and Sontheimer, E.J. (2015). DNase H activity of *Neisseria meningitidis* Cas9. *Mol. Cell* 60, 242–255.

STAR★METHODS

KEY RESOURCES TABLE

REAGENT or RESOURCE	SOURCE	IDENTIFIER
Chemicals, Peptides, and Recombinant Proteins		
T7 Endonuclease 1	New England Biolabs	#M0302L
NcoI-HF	New England Biolabs	#R3193S
HindIII-HF	New England Biolabs	#R3104S
Sall	New England Biolabs	#R0138S
XhoI	New England Biolabs	#R0146S
BsmBI	New England Biolabs	#R0580S
BstBI	New England Biolabs	#R0519S
Scal-HF	New England Biolabs	#R3122S
Tobacco Etch Virus (TEV) protease	A. Davidson Lab	N/A
Ni-NTA agarose resin	QIAGEN	#30210
cOmplete, Mini, EDTA-free Protease Inhibitor Cocktail	Sigma Aldrich	#11836170001
DNeasy Blood and Tissue Kit	QIAGEN	#69504
QIAamp DNA Mini Kit	QIAGEN	#51304
GC Medium Base	Difco	#DF0289-17-3
DMEM (Medium for mammalian cell culture)	GIBCO	#11965092
Fetal Bovine Serum (For mammalian cell culture)	Sigma Aldrich	#F4135
Penicillin-Streptomycin (For mammalian cell culture)	Sigma Aldrich	#P4333
High Fidelity 2X PCR Master Mix	New England Biolabs	#M0541S
PolyFect transfection reagent	QIAGEN	3011
AmpliScribe T7-Flash Transcription kit	Epicenter	ASF3507
Gibson Assembly Master mix	New England Biolabs	E2611S
Experimental Models: Cell Lines		
Human: HEK293T	ATCC	ATCC CRL-3216
Human: U2OS	ATCC	ATCC HTB96
Experimental Models: Organisms/Strains		
<i>Neisseria meningitidis</i> strain 8013	E. Sontheimer Lab	N/A
<i>Escherichia coli</i> Rosetta (DE3)	Thermo Fisher Scientific	# 709544
<i>Escherichia coli</i> BL21 (DE3)	A. Davidson Lab	N/A
Recombinant DNA		
pGCC2	Zhang et al., 2013	N/A
pGCC2/ <i>P</i> _{cas9} +AcrIIC1 _{Boe} (For strain <i>nics</i> :: <i>P</i> _{cas9} - <i>acrIIC1</i> _{Boe})	This study	N/A
pGCC2/ <i>P</i> _{cas9} +AcrIIC1 _{Nme} (For strain <i>nics</i> :: <i>P</i> _{cas9} - <i>acrIIC1</i> _{Nme})	This study	N/A
pGCC2/ <i>P</i> _{cas9} +AcrIIC2 _{Nme} (For strain <i>nics</i> :: <i>P</i> _{cas9} - <i>acrIIC2</i> _{Nme})	This study	N/A
pGCC2/ <i>P</i> _{cas9} +AcrIIC3 _{Nme} (For strain <i>nics</i> :: <i>P</i> _{cas9} - <i>acrIIC3</i> _{Nme})	This study	N/A
pHAT4	Peränen et al., 1996	N/A
pHAT4-AcrE2	This study	N/A
pHAT4-AcrIIC1 _{Boe}	This study	N/A
pHAT4-AcrIIC1 _{Nme}	This study	N/A
pHAT4-AcrIIC2 _{Nme}	This study	N/A
pHAT4-AcrIIC3 _{Nme}	This study	N/A
pEJS561:sgRNA (see pEJS561 below)	This study; derived from Zhang et al., 2015	N/A
pEJS560 (Protospacer 25 in pUC19)	E. Sontheimer Lab	N/A

(Continued on next page)

Continued

REAGENT or RESOURCE	SOURCE	IDENTIFIER
pEJS561 (6XHis-TEV-WtNmeCas9 in pMCSG7)	Zhang et al., 2015	N/A
pEJS24 (pCSDest2-SpyCas9-NLS-3XHA-NLS)	S. Wolfe Lab	Addgene #69220
pEJS424 (pCSDest2-NmeCas9-NLS-3XHA-NLS)	E. Sontheimer Lab	N/A
pEJS427 (pCSDest2-AcrE2)	This study	N/A
pEJS430 (pCSDest2-AcrIIC1 _{Boe})	This study	N/A
pEJS433 (pCSDest2-AcrIIC1 _{Nme})	This study	N/A
pEJS436 (pCSDest2-AcrIIC2 _{Nme})	This study	N/A
pEJS443 (pCSDest2-AcrIIC3 _{Nme})	This study	N/A
pEJS333 (pLKO.1-puro U6 Nme-sgRNA BfuAI stuffer)	S. Wolfe Lab	N/A
pEJS334 (pLKO.1-puro U6 Spy-sgRNA BfuAI stuffer)	S. Wolfe Lab	Addgene #52628
pEJS15 (pSimpleII-NmeCas9-sgRNA/Empty)	E. Sontheimer Lab	N/A
pEJS466 (pHAGE-TO-Nme dCas9-3xGFP)	Addgene #64109	N/A
pEJS467 (pHAGE-TO-Spy dCas9-3xmCherry)	Addgene #64108	N/A
pEJS468 (pLK.O1-NmeSgRNA/DTS13-Telomere)	This study	N/A
pEJS469 (pLK.O1-SpySgRNA/DTS13-Telomere)	This study	N/A
pEJS476 (pHAGE-TO-Nme dCas9 3XGFP-SgRNA/Telomere-All-in-one)	This study	N/A
pEJS477 (pHAGE-TO-Spy dCas9 3XmCherry-SgRNA/Telomere-All-in-one)	This study	N/A
pEJS478 (pIRES-mTagBFP2)	D. Grünwald Lab	N/A
pEJS507 (pCDEST2-noAcr-mTagBFP2-IRES)	This study	N/A
pEJS481 (pCDEST2-AcrE2-mTagBFP2-IRES)	This study	N/A
pEJS482 (pCDEST2-AcrIIC3 _{Nme} -mTagBFP2-IRES)	This study	N/A
Sequence-Based Reagents		
sgRNA for coexpression with NmeCas9 (used to create pEJS561:sgRNA) 5'-TGAGACCAGTCTCGGAAGCTCAAAGGTCTC GTTGTAGCTCCCTTCTC ATTTTCGAAACGAAATGAGAACCGTTGCTACAATAAGGCCGTCTGAAAAG ATGTGCCGCAACGCTCTGCCCTTAAAGCTTCTGCTTTAAGGGGCATCGT TTATTTTCGTTAAAAAATGCCGT-3'	Genscript	N/A
See Table S3 for sequences of oligonucleotides used in this study		
Software and Algorithms		
FastTree	Adam Arkin's Lab	http://www.genome.jp/tools/fasttree/
ImageMaster TotalLab V2.0	TotalLab	http://totalab.com/

CONTACT FOR REAGENT AND RESOURCE SHARING

Further information and requests for resources and reagents should be directed to Lead Contact Alan R. Davidson (alan.davidson@utoronto.ca).

EXPERIMENTAL MODEL AND SUBJECT DETAILS

***Neisseria meningitidis* strain 8013**

Strains were grown on GC Medium Base (GCB) plates with Kellogg's supplements (22.2 mM glucose, 0.68 mM glutamine, 0.45 mM cocarboxylase, 1.23 mM Fe(NO₃)₃, all from Sigma), with or without appropriate antibiotics (chloramphenicol, 2.5 μg/mL, erythromycin 2.5 μg/mL, both from Sigma). All solid cultures were incubated at 37°C in a 5% CO₂ humidified atmosphere.

***Escherichia coli* Rosetta (DE3)**

E. coli Rosetta (DE3) cells were used for protein expression for in vitro studies. Cells were grown at 37°C (unless otherwise indicated) in Terrific Broth (TB) medium supplemented with 34 μg/mL chloramphenicol, and, when appropriate, 100 μg/mL ampicillin for plasmid maintenance.

Escherichia coli BL21 (DE3)

This strain was used for recombinant anti-CRISPR protein expression for downstream use in *in vitro* assays. Cells were grown at 37°C (unless otherwise indicated) in LB medium supplemented with 100 µg/mL ampicillin for plasmid maintenance.

HEK293T

Cells were cultured in 10 cm culture dish at 37°C, 5% CO₂ in complete DMEM in the presence of 10% FBS and 1% Penicillin/Streptomycin.

U2OS

Cells were cultured in 10 cm culture dish at 37°C, 5% CO₂ in complete DMEM in the presence of 10% FBS and 1% Penicillin/Streptomycin.

METHOD DETAILS

Bioinformatics analysis

BLASTp searches for Aca2 were conducted with WP_019933869.1 from *Oceanimonas smirnovii* as the query (Pawluk et al., 2016). BLASTp searches for Aca3 were conducted with WP_049360086.1 from *Neisseria meningitidis* as the query. For the phylogenetic analysis of Cas9 protein sequences, a list of 257 representative Cas9 protein sequences was extracted from a previous analysis (Fonfara et al., 2014) and updated with newly deposited sequences in the NCBI Protein database. The list was manually trimmed so that only one representative from each species remained. After alignment of the sequences with MUSCLE (Edgar, 2004), FastTree was used to create an unrooted maximum likelihood tree (Price et al., 2009, 2010). Bootstrap values are shown at each node. Based on the data from Fonfara et al. (2014), each clade was classified into subtype II-A (blue), II-B (yellow), or II-C (purple). Clades on the tree are colored in red if they belong to any genus where a validated type II-C anti-CRISPR gene or its homolog was found. Some noteworthy Cas9 proteins are highlighted on the tree by asterisks.

Plasmid Construction

Acr expression vectors for protein purification

DNA sequences encoding candidate anti-CRISPR proteins were synthesized by GenScript (Piscataway, NJ, USA) and subcloned into pHAT4 (Peränen et al., 1996) using NcoI-HindIII restriction sites. The gene encoding AcrE2 was amplified by PCR from *Pseudomonas* phage JBD88a and ligated into pHAT4 using NcoI-HindIII restriction sites. Table S1 contains the DNA and protein sequences of the anti-CRISPRs tested in this study. AcrIIC3_{Nme} was found to be significantly more soluble upon addition of an N-terminal FLAG tag, so that construct was used for *in vitro* analyses.

Cas9:sgRNA vector for protein purification

DNA encoding a minimal T7 promoter upstream of an sgRNA (with a random sequence, i.e., no genomic target in *E. coli*: 5'-TGAGACCAGTCTCGGAAGCTCAAAGGTCTCGTTGTAGCT CCCTTTCTCATTTTCGGAACGAAATGAGAACCGTTGCTACAATAAGGCCGTCTGAAAAGATGTGCCGCAACGCTCTGCCCTTAAAGCTTCTGCTTTAAGGGGCATCGTTATTTTCGGTAAAAAATGCCGT-3') was synthesized by GenScript (Piscataway, NJ, USA). This insert was cloned into the previously described pMCSG7-NmeCas9 expression vector (Zhang et al., 2015), downstream of the NmeCas9 protein-coding region, into the Sall-XhoI restriction sites.

Cas9/sgRNA mammalian expression vectors

For editing of DTS3 and DTS7 by both SpyCas9 and NmeCas9 (Figures 4, S3, and S4), we used Cas9 expression vectors that were identical in all respects [plasmid backbone, CMV IE94 promoter (Villefranc et al., 2007), UTRs, terminal fusions of NLSs and epitope tags, etc.] except for the respective Cas9 ORFs. The SpyCas9 expression plasmid (pEJS24) has been described previously (Bolukbasi et al., 2016) and the NmeCas9 expression plasmid (pEJS424) was generated from (pEJS24) by Cas9 ORF replacement via Gibson assembly (New England Biolabs). Similarly, plasmids for the expression of sgRNAs for each Cas9 ortholog were also identical in all respects except for the sgRNA sequences themselves. The SpyCas9 sgRNA plasmid pLKO.1-puro has been described previously (Kearns et al., 2014), and the NmeCas9 sgRNA expression plasmid (pEJS333) was generated from it by Gibson assembly. The plasmids expressing NmeCas9 and its sgRNA are described in detail elsewhere (N.A., X.D. Gao, L.J. Zhu, S.A. Wolfe, and E.J.S, unpublished data).

For editing of the N-TS1C, N-TS4B, N-TS4C, N-TS7, N-TS8, N-TS11 and N-TS25 sites (Figure S3), we used an all-in-one vector (pEJS15) expressing both NmeCas9 (under the control of the EF-1 α promoter) and its sgRNA (under the control of the U6 promoter). This plasmid, which was derived from pSimplell (Hou et al., 2013), is also described elsewhere (N.A., X.D. Gao, L.J. Zhu, S.A. Wolfe, and E.J.S, unpublished data). The 24-nt guide sequences for each distinct target site (see Figure S3B and STAR Methods for target site sequences) were inserted into the sgRNA cassette of pEJS15 by the ligation of synthetic oligonucleotide duplexes into its *BsmBI* sites.

Acr vectors for mammalian expression

To generate the Acr expression plasmids p427-AcrE2, p430-AcrIIC1_{Boe}, p433-AcrIIC1_{Nme}, p436-AcrIIC2_{Nme}, and p443-AcrIIC3_{Nme}, each ORF was synthesized as a gene block (Integrated DNA Technologies) flanked by *XhoI* and *BstBI* sites, with a Kozak consensus sequence upstream of the initiation codon. The synthetic Acr sequences (provided in Table S1) were then inserted into the *XhoI* and

*Bst*BI sites of the pCS2-Dest vector (Addgene). The resulting plasmids placed the Acr-encoding genes under the control of the CMV IE94 promoter.

Vectors for fluorescence microscopy

pHAGE-TO-DEST dSpyCas9-(mCherry)₃ and dNmeCas9-(sfGFP)₃ plasmids (Ma et al., 2015b) were purchased from Addgene (#64108 and #64109, respectively) and used directly for no-sgRNA control experiments. We also modified each into an all-in-one version (pEJS466 and pEJS467, respectively) that also included an sgRNA-expressing cassette, with the sgRNAs targeted to telomeric repeats. For the latter, we first used the SpyCas9 sgRNA vector pLKO.1-puro (see above; Kearns et al., 2014) and the NmeCas9 sgRNA vector pEJS333 (see above) to generate the telomere-targeting sgRNAs, via insertion of synthetic oligonucleotide duplexes. We then inserted each U6 promoter/sg-telomere cassette into its cognate dCas9 plasmid via Gibson assembly to generate all-in-one plasmids, pEJS476 [for dNmeCas9-(sfGFP)₃] and pEJS477 [dSpyCas9-(mCherry)₃]. To make the Acr plasmids, we amplified an mTagBFP2 cassette and incorporated it into pEJS427 (expressing AcrE2) and pEJS443 (expressing AcrIIIC3_{Nme}) by Gibson assembly, yielding pEJS481 and pEJS482, respectively. To generate the control plasmid that lacks any Acr (pEJS507), we removed the AcrIIIC3_{Nme} cassette from pEJS482 by XhoI digestion followed by plasmid backbone purification and re-ligation.

Neisseria meningitidis natural transformation

Candidate anti-CRISPR genes with the native NmeCas9 promoter and Shine-Dalgarno sequence were cloned into pGCC2, a *N. meningitidis* vector containing homology arms for integration of the insert into the *N. meningitidis* chromosome at the *nics* locus, as described previously (Zhang et al., 2013). The pGCC2 constructs were transformed into *N. meningitidis* strain 8013, and erythromycin-resistant transformants were selected. Two or three representative transformants per reaction were verified by re-streaking on selective plates twice and then confirmed by PCR on purified genomic DNA. This procedure resulted in *N. meningitidis* strain 8013 derivatives with chromosomally integrated anti-CRISPR genes under the control of the native promoter of *N. meningitidis* Cas9. In all cases, we sequence-confirmed the CRISPR locus in the derived strains to ensure that the spacers to be tested for interference activity were intact. Transformation assays to assess CRISPR-Cas activity of these strains were completed as described previously (Duffin and Seifert, 2012; Zhang et al., 2013), with protospacer 25 (complementary to the crRNA derived from endogenous CRISPR spacer #25) as the target. Briefly, 150 ng of plasmids were used per transformation reaction and 10 μ L of serial 10-fold dilutions were spotted on GCB plates in triplicate in the presence and absence of appropriate antibiotics. 200 μ L from the undiluted final transformation mixture were also plated on GCB plates with appropriate antibiotics to enhance detection. Eight representative transformants per reaction were verified by re-streaking on selective plates twice and then verified by PCRs on cell extracts. Transformation frequencies were reported as antibiotic-resistant cfu/mL from at least three independent experiments (mean \pm SEM).

Cloning and purification of anti-CRISPR proteins

Anti-CRISPRs were purified from pHAT4 constructs expressed in *E. coli* BL21 (DE3) as described previously (Bondy-Denomy et al., 2015). After elution from Ni-NTA resin, anti-CRISPR proteins were dialyzed in 10 mM Tris pH 7.5, 250mM NaCl, and 5mM β -mercaptoethanol and incubated with His-tagged Tobacco Etch Virus (TEV) protease overnight at 4°C. A second round of Ni-NTA purification was used to isolate successfully cleaved, untagged anti-CRISPRs by collecting the unbound fraction.

Purification of Cas9

6xHis-NmeCas9:sgRNA was expressed in *E. coli* Rosetta (DE3). Cells were grown in Terrific Broth (TB) medium at 37°C to an optical density (OD_{600 nm}) of 0.8 in the Lex Bubbling System (Structural Genomics Consortium, Toronto, Canada). Protein expression was induced by the addition of 1 mM IPTG for 16 hr at 16°C. Cells were lysed by sonication in 50 mM Tris pH 7.5, 500 mM NaCl, 20 mM imidazole, 0.5 mM DTT and 5% glycerol supplemented with 0.5 mM PMSF, lysozyme and protease inhibitor cocktail (Sigma). Clarified lysates were bound in batch to Ni-NTA agarose (QIAGEN), and bound protein was eluted with 300 mM imidazole. Purified Cas9:sgRNA was dialyzed into 20 mM HEPES pH 7.5, 250 mM NaCl, 5% glycerol, 1 mM DTT and 1 mM PMSF) for protein interaction experiments. 6xHis-MBP-tagged AnaCas9 was purified from *E. coli* Rosetta (DE3) cells as described previously (Ma et al., 2015a).

Cas9-anti-CRISPR pulldown assays

Untagged anti-CRISPR proteins (after TEV cleavage) were incubated with and without NmeCas9 for 1 hr at 4°C in binding buffer (20 mM HEPES pH 7.5, 250 mM NaCl, 5% glycerol, 5 mM imidazole), and input fractions were set aside for SDS-PAGE analysis. 50 μ L 50% slurry Ni-NTA beads were added to each tube. After 30 min incubation at 4°C with rotation, the beads were collected by centrifugation at 3000 rpm for 2 min. Beads were washed four times with 1 mL binding buffer supplemented with 20 mM imidazole and collected by centrifugation. Bound proteins were eluted with elution buffer (binding buffer containing 300 mM imidazole). The input and elution fractions were analyzed by SDS-PAGE followed by Coomassie staining.

In vitro DNA cleavage

NmeCas9 sgRNA derived from spacer 25 (Zhang et al., 2015) was generated by in vitro T7 transcription (Epicenter). NmeCas9 (500 nM) was incubated with purified, recombinant anti-CRISPR protein in cleavage buffer [20 mM HEPES-KOH (pH 7.5), 150 mM KCl, 10% glycerol, 1 mM DTT, and 10 mM MgCl₂] for 10 min. Next, sgRNA (1:1, 500 nM) was added and the mixture was incubated for another 15 min. Plasmid containing the target protospacer 25 (pEJS560) was linearized by Scal digestion.

Linearized plasmid was added to the Cas9/sgRNA complex at ~5 nM final concentration. The reactions were incubated at 37°C for 30 min and visualized after electrophoresis in a 1% agarose/1xTAE gel.

Mammalian genome editing

Plasmids for mammalian expression of NmeCas9, SpyCas9, their respective sgRNAs, and the anti-CRISPR proteins are listed in [STAR Methods](#). Approximately 1.5×10^5 mid-passage HEK293T cells [cultured at 37°C, 5% CO₂ in DMEM (GIBCO) + 10% FBS(Sigma) + 1% Penicillin/Streptomycin (Sigma)] were transiently transfected with 150 ng Cas9-expressing plasmid and 150 ng sgRNA-expressing plasmid, using Polyfect transfection reagent (QIAGEN) in 24-well plates according to the manufacturer's instructions. Alternatively, 200 ng of an all-in-one plasmid expressing both NmeCas9 and the appropriate sgRNA (see the [STAR Methods](#)) was used for transfection. For experiments that included Acr protein expression, 100 ng of the Acr plasmid was included in the co-transfection mix.

72 hr after transfection, cells were harvested and genomic DNA was extracted with the DNeasy Blood and Tissue kit (QIAGEN) according to the manufacturer's instructions. 50 ng genomic DNA was used for PCR amplification [High Fidelity 2X PCR Master Mix (New England Biolabs)] with primers flanking the targeted site. 10 μ l of each PCR product was heat-denatured, re-annealed, and digested with T7 Endonuclease I (New England Biolabs). The samples were fractionated in a 2.5% agarose/1xTAE gel and quantified with the ImageMaster-TotalLab program. Indel percentages (“% lesion” in the figures) were calculated as previously described ([Guschin et al., 2010](#)).

Fluorescence microscopy of dNmeCas9

U2OS cells were cultured at 37°C (5% CO₂) in DMEM (GIBCO) supplemented with 10% FBS (Sigma) and 1% Pen/Strep (Sigma). For imaging, cells were grown on 170 μ m, 35 \times 10mm glass-bottom dishes (Eppendorf). Cells were cotransfected with 300 ng of all-in-one plasmids (150 ng of each dNmeCas9 and dSpyCas9 plasmid), an additional 600 ng of sgRNA-expressing plasmids, and 100ng of anti-CRISPR/mTagBFP2 plasmid using PolyFect (QIAGEN) according to the manufacturer's instructions. The additional sgRNA-only plasmid was included because we found the levels of sgRNAs expressed from the all-in-one plasmid alone to be subsaturating, relative to the amount of dCas9 that was expressed from the same plasmid. For the no-sgRNA control experiments, the additional sgRNA-only plasmids were excluded, and the sgRNA cassette was also excluded from the cognate dCas9-expressing plasmid. The total amount of DNA was equal in all transfections (e.g., for the no-sgRNA controls, the sgRNA-expressing plasmids were replaced with the same mass of an irrelevant plasmid). After 24 hr of incubation, live cells were imaged with a Leica DMI8 microscope equipped with a Hamamatsu camera (C11440-22CU), a 63x oil objective lens, and Microsystems software (LASX). Further imaging processing was done with Fiji-ImageJ. For the “blind” experiments ([Figure 5G](#)), cells from each condition were coded by one experimenter and then scored by another who did not know which set of cells were from which condition. Only cells that exhibited mTagBFP2 and sfGFP fluorescence as well as dSpyCas9-(mCherry)₃ telomeric foci were assessed for the presence or absence of co-localizing dNmeCas9-(sfGFP)₃ telomeric foci, and all such imaged cells were included in the quantifications.

QUANTIFICATION AND STATISTICAL ANALYSIS

Neisseria meningitidis transformation efficiency

Cfu/mL were counted manually and are reported as the mean \pm s.e.m of at least three biological replicates.

Genome editing efficiency

Efficiency of genome editing in mammalian cells was calculated based on fraction of cleaved DNA as detected by ImageMaster TotalLab V2.0.

$$\% \text{ efficiency} = 1 - \sqrt{1 - \text{fraction}_{\text{cleaved}}}$$

The gel images shown for these experiments are representative of at least seven replicates.

Fluorescence imaging

Blind scoring was performed by having one researcher label plates of cells from each condition arbitrarily. A second researcher then collected and scored the images for presence of telomeric foci, and then the labels were decoded to yield the data presented in [Figure 5G](#). These measures were taken to avoid bias. All imaged cells that exhibited mTagBFP2 and sfGFP fluorescence as well as dSpyCas9-(mCherry)₃ telomeric foci were included in the quantification. In [Figure 5G](#), n refers to the total number of cells that were scored in each indicated condition.

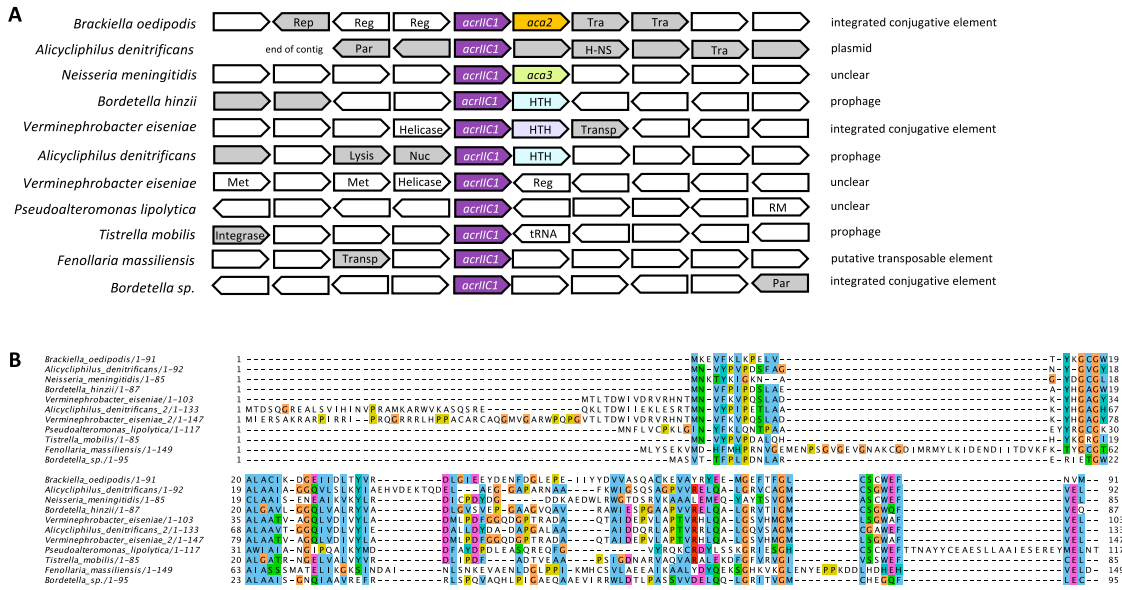


Figure S1. AcrIIc1 Putative Orthologs Are Widely Dispersed in MGEs of Different Species, Related to Figure 1 and Table S2

(A) Schematic representation of AcrIIc1 putative orthologs identified by PSI-BLAST and their genomic contexts. The species in which each is found and its predicted genomic region classification (i.e., prophage, integrated conjugative element) are indicated. Gene arrows are not drawn to scale. Grey arrows represent genes that have a clear connection to mobile DNA; either by function (i.e., integrase) or by evidence of horizontal transfer as determined by BLAST search. Known, relevant gene functions are indicated by labels: Rep, plasmid replication protein; Reg, transcriptional regulator; Tra, conjugal transfer protein; Par, plasmid partitioning protein; H-NS, histone-like nucleoid-structuring protein; HTH, helix-turn-helix DNA-binding protein; Transp, transposase; Lysis, phage lysis cassette; Nuc, nuclease; Met, methyltransferase; RM, restriction-modification system.

(B) Protein alignment of AcrIIc1 homologs identified by PSI-BLAST searches, using the ClustalX color scheme.

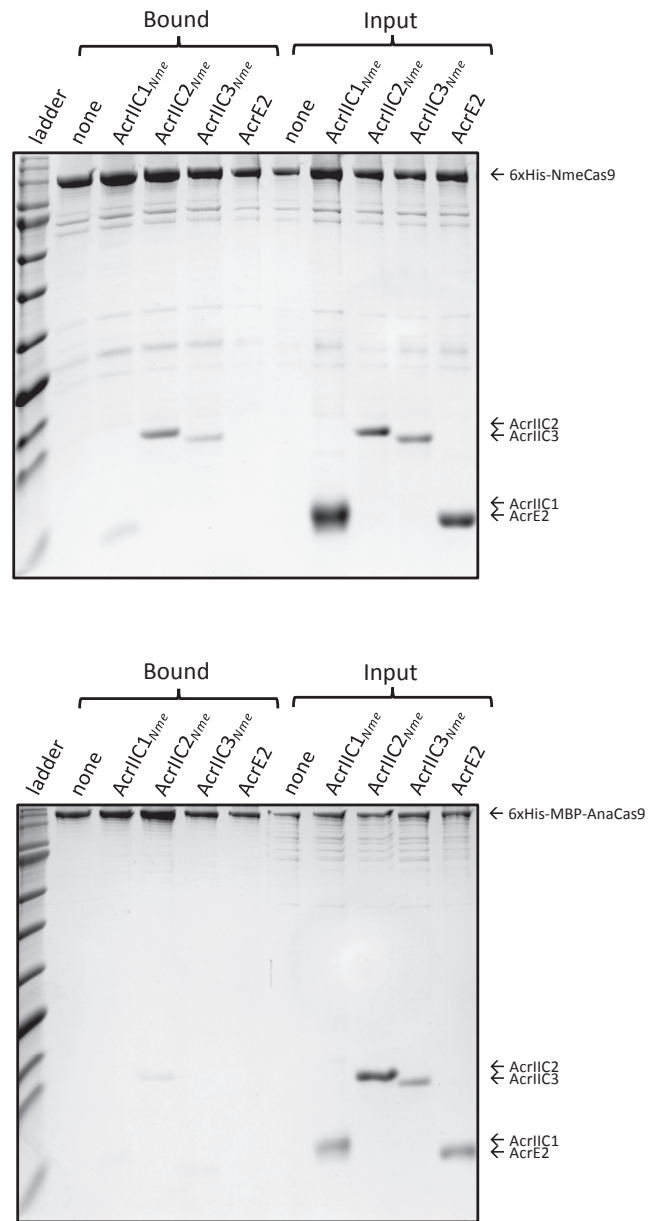
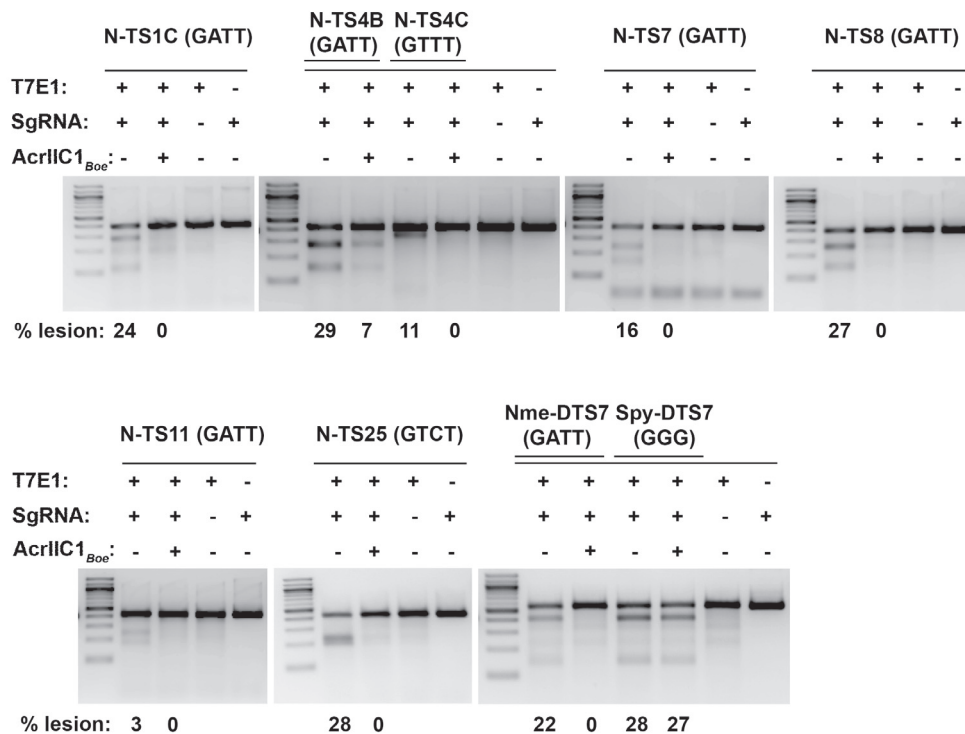


Figure S2. Anti-CRISPRs Interact Specifically with NmeCas9, Related to Figure 2
Uncropped images of the Coomassie-stained SDS-PAGE analysis from Figure 2 are shown.

A



B

Site	Gene or locus	Spacer sequence	Target site
N-TS1C	SLC9A9	GUGGUCUGGGUACAGCCUUGGCA	TACTTGGTCTGGGGTACAGCCTTGGCA <u>CATGATT</u> TTG
N-TS4B	FLJ00328	GGACAGGAGUCGCCAGAGCCGGU	GCAGGACAGGAGTCGCCAGAGCCGGT <u>GGTGGATT</u> TCC
N-TS4C	FLJ00328	GGGGCUGGCCUCCAGUCGCCCGC	TGCGGGGCTGGCTCCACGTGCGCCCG <u>GGCGGTT</u> GGG
N-TS7	LOC100505797	GAGGGAGAGAGGUGAGCGGAUGAA	GCAAAGGGAGAGAGGTGAGCGGATGA <u>GGGAGATT</u> GGT
N-TS8	ESPN	GGACGCAAUUCCAGAGGUGAUGGG	CGGCGACGCAATTCCAGAGGTGATGGG <u>GAGTATT</u> GTC
N-TS11	SMARCB1	GUUCCAGUUGGGAAGGCCAGUGC	TAGATTCCAGTTGGAAGGGCCAGTG <u>CCTCCGATT</u> CCA
N-TS25	AC193513	GGUUUCUCAUCCUGUCUUCUGCCU	CCGCGTTTCTCATCTGTCTTCTGCCT <u>AGTGGAT</u> ATGT
Nme-DTS3	ARHGEF9	GACUGAAGGCGAGGUCCGGGGCGG	GACTGAAGGCGAGGTCCGGGGCGG <u>AGGGGATT</u> GGG
Spy-DTS3	ARHGEF9	GAAGGCGAGGUCCGGGGCGG	GACTGAAGGCGAGGTCCGGGGCGG <u>AGGGGATT</u> GGG
Nme-DTS7	LSP1	GGCUGGCACCCUCCAUGUACCCAG	GGCTGGCACCCCTCATGTACCCAG <u>GGGAGATT</u> CCA
Spy-DTS7	LSP1	GGCACCCUCCAUGUACCCAG	GGCTGGCACCCCTCATGTACCCAG <u>GGGAGATT</u> CCA

Figure S3. AcrIIC1_{B_{oe}} Blocks NmeCas9-Mediated Genome Editing at Multiple Human Genome Sites, Related to Figure 4 and Table S3

(A) T7E1 assays of NmeCas9 editing efficiencies at multiple sites, with canonical (N₄GATT) or variant (N₄GTTT, N₄GTCT) PAMs, upon transient transfection of human HEK293T cells. Plasmid encoding AcrIIC1_{B_{oe}} proteins was co-transfected as indicated at the top of each lane. For the D-TS7 target site, SpyCas9 editing (with and without AcrIIC1_{B_{oe}}) was also tested. Editing efficiencies (“% lesion”) are given at the bottom of each lane.

(B) For the D-TS3 site tested in Figure 4 and for each site tested in (A), the NmeCas9 sgRNA spacer sequences (5′ to 3′) and DNA target sites (non-complementary strand, 5′ to 3′) are listed.

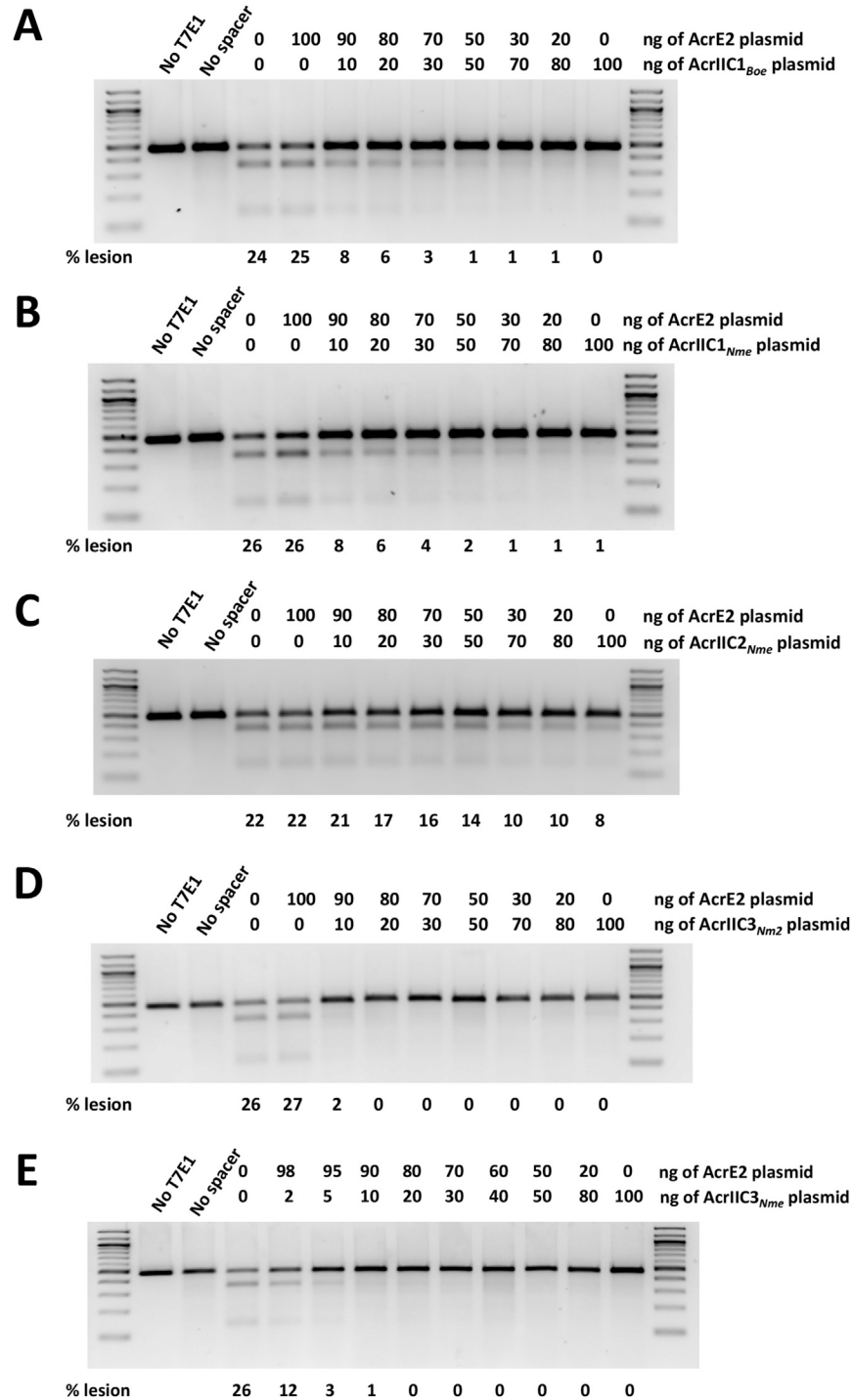


Figure S4. Plasmid Titration of Anti-CRISPRs in Human Genome Editing, Related to Figure 4

(A) T7E1 assays of NmeCas9 editing efficiencies at DTS3 upon transient transfection of human HEK293T cells. Constructs encoding anti-CRISPRs were co-transfected as indicated at the top of each lane. The total amount of anti-CRISPR plasmid was held constant at 100 ng per well, but the relative amount of a negative control anti-CRISPR (AcrE2) and test anti-CRISPR (AcrIIC1_{Boe}) was varied. Editing efficiencies (“% lesion”) are given at the bottom of each lane.

(B–E) As in (A), except that AcrIIC1_{Nme} (B), AcrIIC2_{Nme} (C), and AcrIIC3_{Nme} (D and E) were used. In (D), because inhibition was nearly complete even at the lowest dose (10 ng) of AcrIIC3_{Nme} plasmid, we repeated the titration with lower levels of plasmid in (E), revealing the dose-dependence of inhibition.